

DEM HEAT TRANSFER MODELS

Rafael López Rangel
(rrangel@cimne.upc.edu)

Summary

1 – Introduction

[1.1 – Lumped Capacitance Analysis](#)

[1.2 – Calculation Cycle](#)

[1.3 – Coupled Problem](#)

[1.4 – Time Step Size](#)

[1.5 – Heat Transfer Mechanisms](#)

[1.6 – Motion of Granular Materials](#)

[1.7 – Mechanisms Contributions](#)

2 – Conductive Heat Transfer

[2.1 – Heat Conduction Mechanisms](#)

[2.2 – Collisional Contact Models](#)

[2.3 – Static Contact Models](#)

[2.4 – Thermal Network Models](#)

[2.5 – Voronoi-Based Models](#)

[2.6 – Surrounding Layer Models](#)

[2.7 – Other Conduction Models](#)

[2.8 – Low Stiffness Correction Models](#)

3 – Convective Heat Transfer

[3.1 – Heat Convection Mechanisms](#)

[3.2 – Dimensionless Numbers](#)

[3.3 – Convection Correlations](#)

[3.4 – Calculation Procedure](#)

4 – Radiative Heat Transfer

[4.1 – Heat Radiation Mechanisms](#)

[4.2 – DEM Radiation Models](#)

5 – Heat Generation

Appendix A – Contact Mechanics

Nomenclature

Bibliography

1 – Introduction

Thermomechanical Simulation

Besides mechanical energy, DEM particles can also exchange thermal energy.

Mechanical energy exchange

Leads to the resulting force and torque acting upon a particle, which is responsible for its motion (displacements and rotations)

Thermal energy exchange

Leads to the net heat flux towards or outwards a particle, which is responsible for its temperature variation

This document shows heat transfer models for soft-sphere DEM (Cundall & Strack, 1979) considering round-shaped particles: 2D discs or 3D spheres

Lumped Capacitance Analysis

Biot number

Dimensionless number that gives the ratio of the heat transfer resistance by conduction inside the body and by convection on its surface:

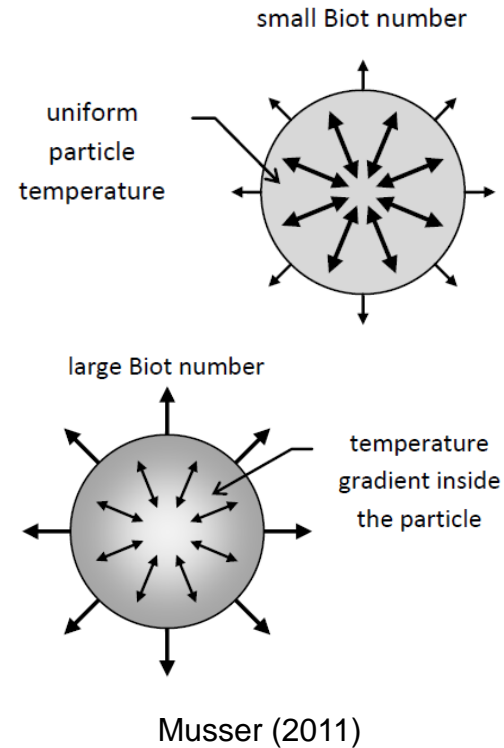
$$Bi = \frac{h_i l_i}{k_i}$$

It quantifies the relative importance of conduction and convection to determine whether or not the inner temperature vary significantly in space while it is heated or cooled from a thermal gradient applied to its surface.

Isothermal particles

Valid assumption for thermally thin bodies, in which the *Biot* number is much smaller than unity ($Bi < 0.1$) and the thermal resistance within particles can be neglected.

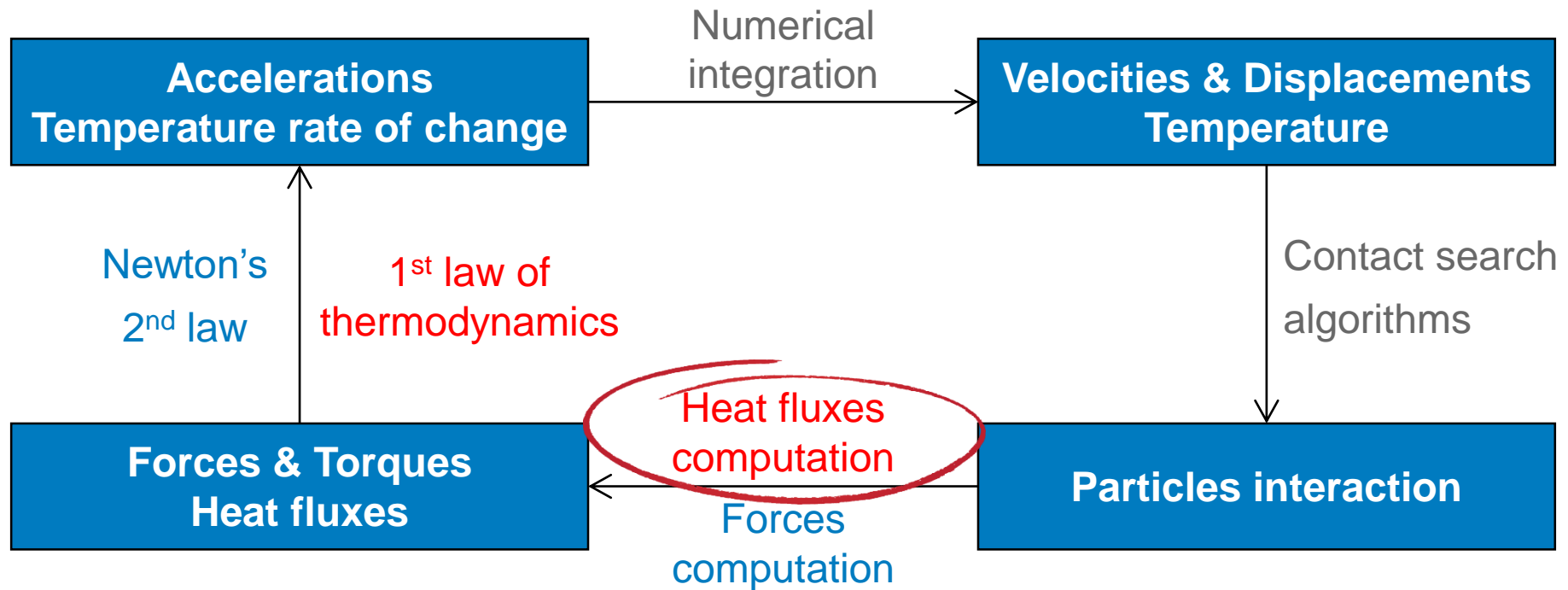
In this case, heat conduction inside the particle is much faster than heat transfer across its surface, so the thermal gradient is negligible and the temperature can be considered as uniform within each particle (Holman, 1981; Incropera, 2006, Cengel, 2007).



Calculation Cycle

Time step cycle

The equations of Newton's 2nd law to obtain the motion of particles remain unchanged, and an additional equation for energy conservation (1st law of thermodynamics) needs to be solved simultaneously to obtain the temperature variation of each particle.



Calculation Cycle

Temperature Calculation

Unsteady equation of energy conservation: $m_i c_i \frac{dT_i}{dt} = Q_i$
(from the 1st law of thermodynamics)

Temperature rate of change: $\frac{dT_i}{dt} = \frac{Q_i}{m_i c_i}$

Numerical integration: $\frac{dT}{dt} = \frac{T^{t+\Delta t} - T^t}{\Delta t}$
(forward Euler scheme)

Temperature evolution: $T_i^{t+\Delta t} = T_i^t + \frac{Q_i^t}{m_i c_i} \Delta t$

Initial condition: $T_i(t = 0) = T_i^0$

Target:

Determine the net rate of heat transferred to each particle in each time step (Q_i^t)!

Coupled Problem

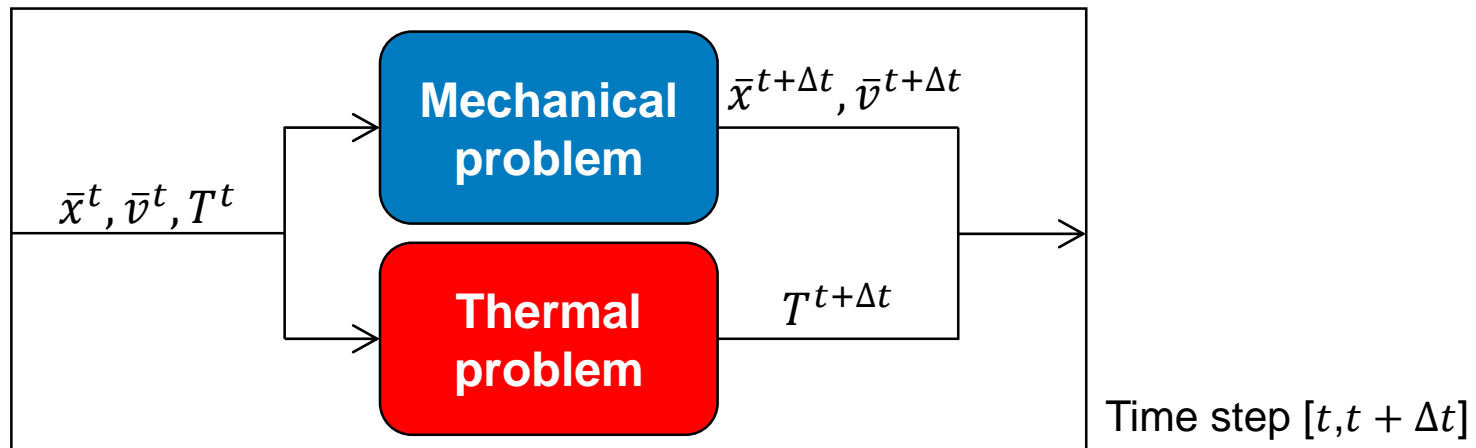
Thermomechanical coupling

The equations of motion and energy conservation are coupled because heat fluxes depend on the kinematics (positions, velocities, etc.), and the mechanical properties can also depend on the temperature.

Coupling scheme

In each time step, the mechanical and thermal problems are solved simultaneously with the position, velocity and temperature from the previous time step.

The mechanical and thermal problems are decoupled within a single time step, so that the solution of one physics does not affect the other during one step.



Time Step Size

Quasi-steady temperature criterion

The size of the time step must be such that the temperature of each particle changes slowly enough so that thermal disturbances do not propagate further than its immediate neighbors during one time step, as with the elastic waves in the mechanical problem (Vargas & McCarthy, 2001).

However, the time step condition for the thermal problem is much less restrictive than for the mechanical problem, hence by ensuring the time integration stability for the mechanical problem automatically ensures the stability for the thermal problem.

The critical time step for the stability of the explicit time integration scheme for the solution of the thermal problem can be estimated by the critical value for the 1D heat conduction problem (Cengel, 2007), and is related to the thermal diffusivity of particles.

Critical time step of thermal problem:
(Rojek, 2014; Moscardini et al, 2018)

$$\Delta t_{cr} = \frac{\rho c R^2}{k}$$

Each particle provides a different value for Δt_{cr} , so the minimum should be considered

Critical time step of mechanical problem:
(Li et al, 2005)

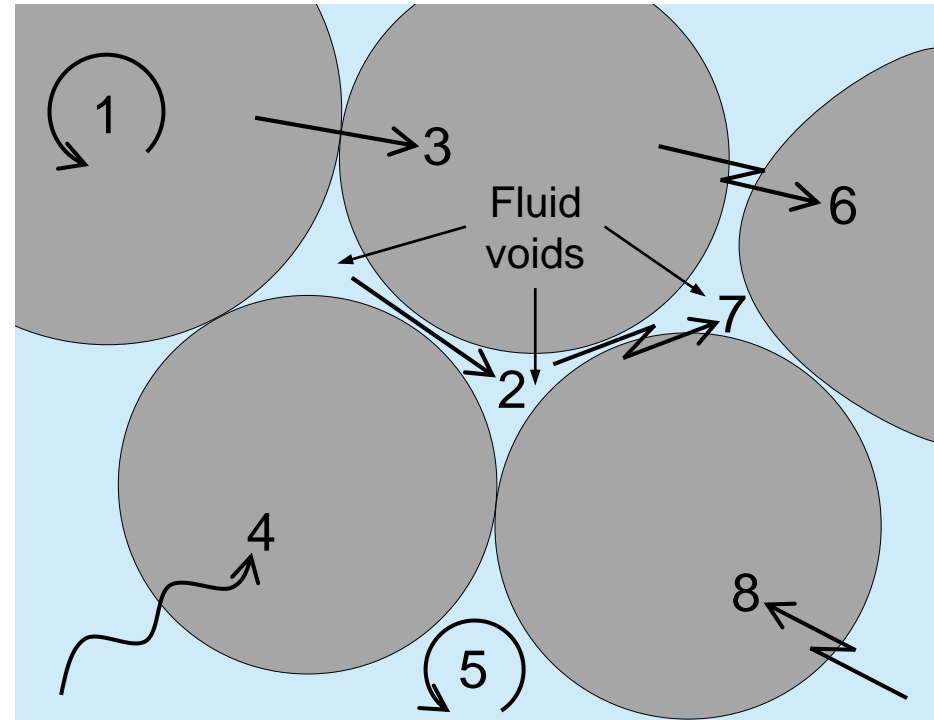
$$\Delta t_{cr} = \frac{\pi R \sqrt{\rho/G}}{0.8766 + 0.163\nu}$$

Heat Transfer Mechanisms

In the presence of a temperature gradient, heat can be transferred by 3 mechanisms:
conduction, convection, radiation.

In fluid-filled packed beds, these mechanisms are identified by (Yagi & Kunii, 1957):

1. **Conduction** within particles
(i.e. non-isothermal particles)
2. **Conduction** between fluid in adjacent voids
(i.e. within the fluid)
3. **Conduction** between particles
(contacted or non-contacted particles)
4. **Convection** between fluid and particles
5. **Convection** within the fluid
6. **Radiation** between particles' surfaces
(in case of interstitial gas)
7. **Radiation** between fluid in adjacent voids
(in case of interstitial gas)
8. **Radiation** between fluid and particles

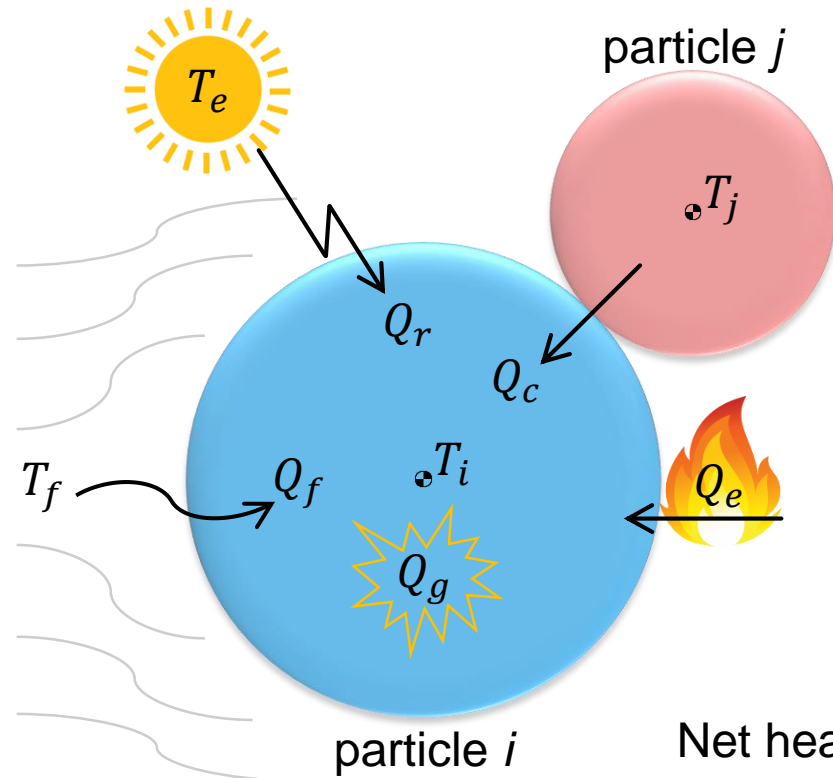


Most DEM simulations only deal with the mechanisms involving the particles. Solving the fluid phase behavior would require a coupled DEM-CFD solution. Focus here on relevant mechanisms for tracking particles temperature (3,4,6).

Mechanism 2:
Cheng et al, 2020

Heat Transfer Mechanisms

Typical components of the net rate of heat transferred to a particle
(positive direction of heat transfer is “entering” the analyzed body – particle i):



- $Q_c \rightarrow$ **Conduction** with neighboring objects
(particles and walls: temperature T_j)
- $Q_f \rightarrow$ **Convection** with surrounding fluid
(temperature T_f)
- $Q_r \rightarrow$ **Radiation** with surrounding environment
(temperature T_e)
- $Q_g \rightarrow$ Heat **generation**
(energy dissipation, chemical reaction, etc)
- $Q_e \rightarrow$ Heat **source**
(fire nozzles, burners, laser beams, etc)

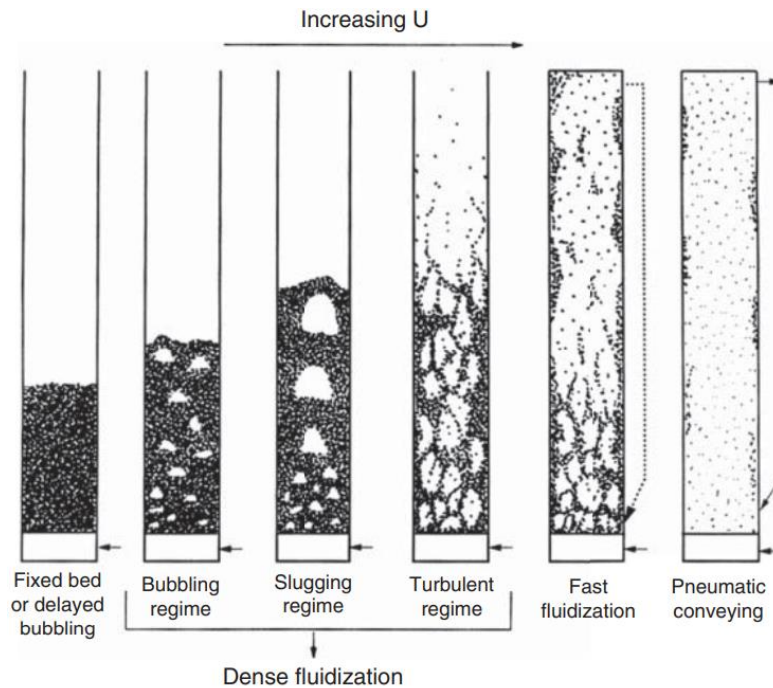
$$\text{Net heat rate: } Q_i = \sum Q_{c,ij} + Q_{f,i} + Q_{r,i} + Q_{g,i} + Q_{e,i}$$

Not all of these mechanisms exist or need to be considered in a specific problem.

Motion of Granular Materials

According to Campbell (2006), all the important granular flows are dense, which means that the particles are constantly in contact with each other, either in a static way or through long-lasting collisions.

However, dilute flows where particle collisions are shorter and less frequent cannot be ignored in the study of heat transfer, as they are part of some industrial application.



Crowe (2006)

For example, in fluidized reactors, depending on the inlet fluid velocity, different regimes might be observed for the granular bed, ranging from a packed bed with no particle motion to a fluidized regime with much less particle contacts.

To account for the fluid motion and temperature, CFD-DEM coupling strategies has been widely used in the study of particle-fluid flow, which is also referred to as Eulerian-Lagrangian methods, but many other coupling strategies can be employed for multiphase flows (Zhu et al, 2007; Wang et al, 2019).

Mechanisms Contributions

Influence of different heat transfer mechanisms

Zhou et al (2009):

Performed CDF-DEM simulations of **packed and fluidized beds**, by using different velocities for the in-flowing gas. The increase of the gas velocity makes the contribution from fluid convection to increase and the conduction to decrease. Under the low temperature conditions (373K), the radiative contribution is very low.

Yang et al (2015):

Performed CDF-DEM simulations of heat transfer in **moving beds** with an inlet gas accounting for conduction, convection and radiation. It shows that particle-fluid convection is dominant with the conduction being much lower and radiation almost insignificant for the considered temperature (although becoming important at higher temperatures).

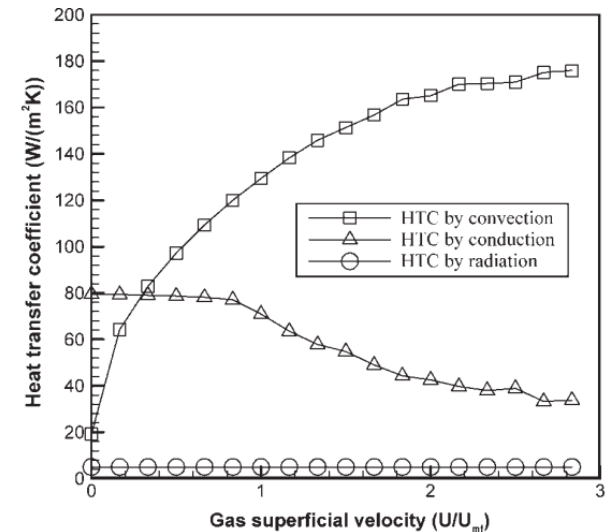
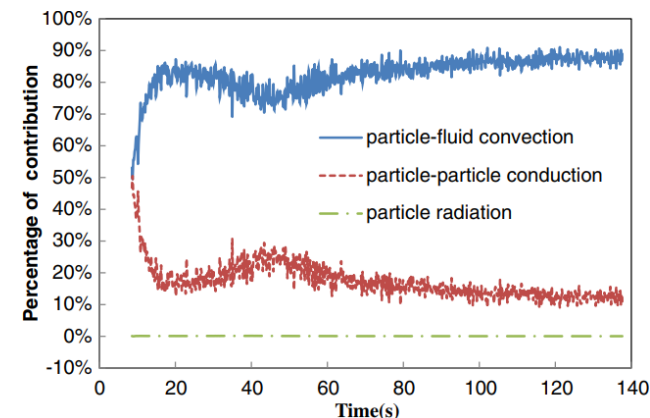


Figure 14. Bed-averaged convective, conductive and radiative heat transfer coefficients (calculated according to Eq. 20a, c and d, respectively) as a function of gas superficial velocity.



Mechanisms Contributions

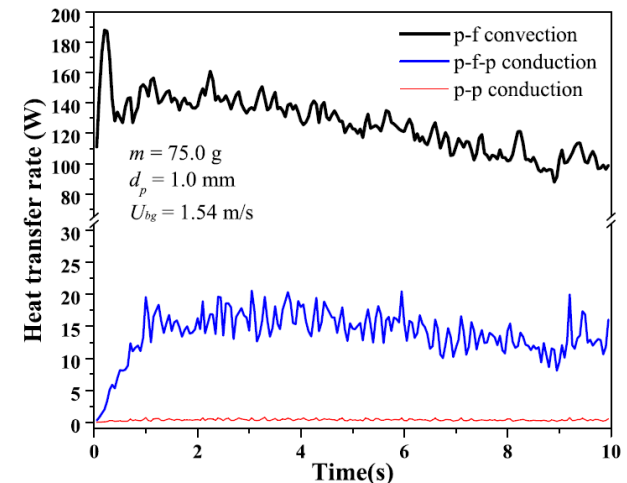
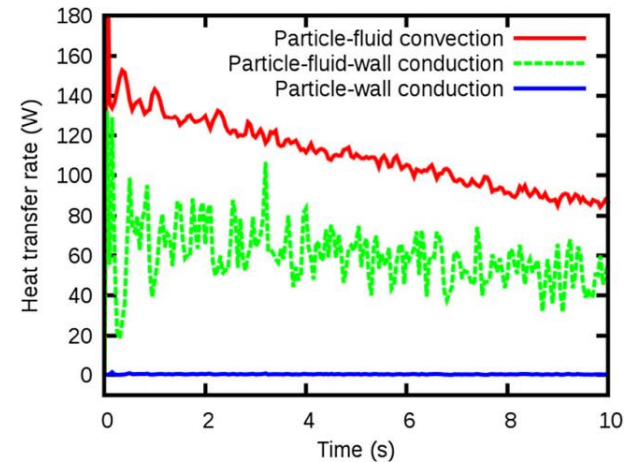
Influence of different heat transfer mechanisms

Lu et al (2017):

Performed coarse grained CFD-DEM simulations of heat transfer in **fluidized beds**, neglecting radiation. Particle-fluid convection accounts for about 65% of the total heat loss while the rest is mainly caused by particle-fluid-wall conduction. The particle-wall contact conduction accounts for less than 1%.

Wang et al (2019):

Performed CFD-DEM simulations of heat transfer in **fluidized beds**, neglecting radiation. The particle-fluid convection dominates the heat transfer while the particle-particle conduction is almost negligible and the particle-fluid-particle conduction occupies about 10% of the total heat transfer.



2 – Conductive Heat Transfer

Heat Conduction Mechanisms

Conductive heat transfer between particles can occur by different mechanisms (Yagi & Kunii, 1957; Cheng et al, 1999):

Direct conduction

Heat conduction through the contact area between two touching particles (contact particle-particle, Q_{cpp})

Indirect conduction

Heat conduction through the fluid in-between two touching particles (contact particle-fluid-particle, Q_{cpfp}), or non-touching particles that are very close (non-contact particle-fluid-particle, Q_{npfp})

The total heat conduction of touching particles is given by the sum of Q_{cpp} and Q_{cpfp} .

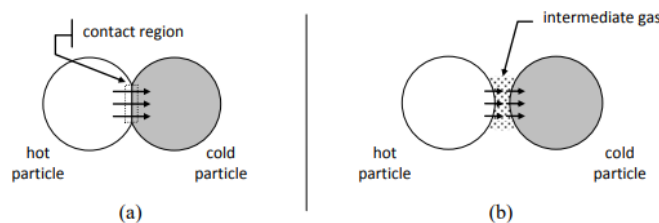
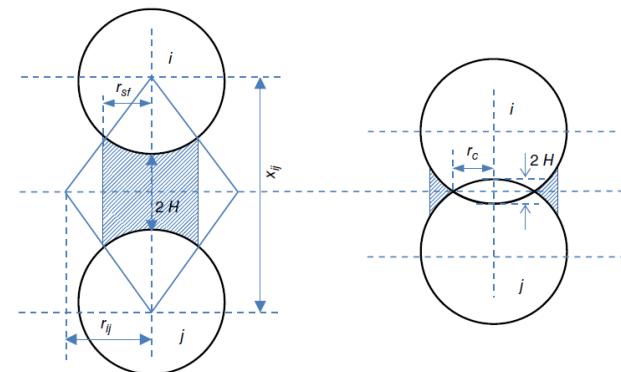


Figure 3-1: Illustration of conduction between particles. (a) *Contact conduction*: thermal energy is transferred from a hot particle to a cold particle through their shared contact area. (b) *Particle-fluid-particle conduction*: thermal energy is transferred from a hot particle to the stagnant gas separating its surface from the cold particle. The thermal energy is then transferred from the stagnant gas to the cold particle.

Musser (2011)



Zhou et al (2009)

Heat Conduction Mechanisms

Indirect conduction

In addition to direct contact conduction (Q_{cpp}), particles may also exchange heat indirectly by the conduction through the thin wedge of interstitial fluid separating their surfaces when they are in close proximity or in contact to one another.

This heat conduction mechanism (generally referred to as Q_{pfp}) is specially important in scenarios where the thermal conductivity of the fluid is comparable to that of the particles (i.e. $k_p R_c / k_f R_i \gg 1$ is not satisfied).



The particle-fluid-particle heat conduction has been studied by several investigators (e.g. Wen & Chang, 1967; Delvosalle & Vanderschuren, 1985; Tsory et al, 2013), but two approaches stand out in the literature, which are described later:

Voronoi-Based Models

Surrounding Layer Models

Heat Conduction Mechanisms

According to Zhou et al (2009), the contribution of each conduction mechanism in packed and fluidized beds is:

- **Non-contact particle-fluid-particle** (triangle):

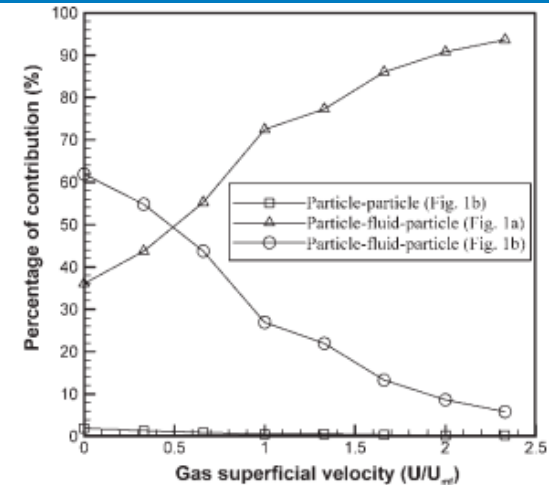
In fluidized beds (x -axis > 1), this mechanism is more relevant than the others for most values of the thermal conductivity of particles.

- **Contact particle-fluid-particle** (circle):

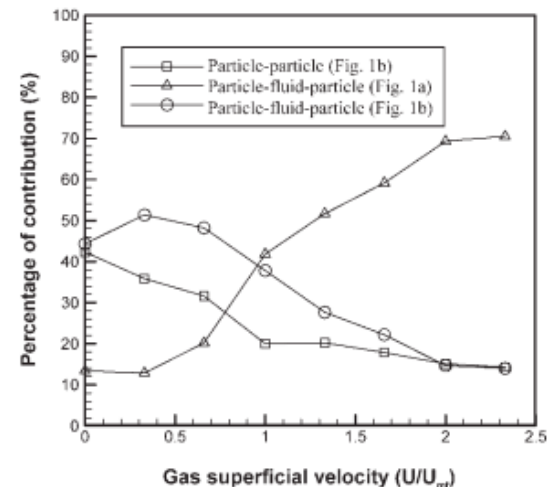
In fixed beds (small values of x -axis), this mechanism is more relevant than non-contact particle-fluid-particle for most values of the thermal conductivity of particles.

- **Contact particle-particle** (square):

Irrelevant for low thermal conductivity of particles ($< 1\%$). For high thermal conductivity, its importance is relevant but decreases from fixed to fluidized beds.



(a)



(b)

Figure 12. Contributions to conduction heat transfer by different heat transfer mechanisms under the condition of (a) $k_p = 0.08 \text{ W/(m}\cdot\text{K)}$, and (b) $k_p = 30 \text{ W/(m}\cdot\text{K)}$.

Heat Conduction Mechanisms

According to Zhou et al (2010) the contribution of each conduction mechanism to the total conduction heat transfer in packed beds with stagnant fluid in-between is described as:

For low thermal conductivity of particles, relative to the interstitial fluid, Q_{cpfp} is dominant. As particle conduction increases, both particle-fluid-particle mechanisms weakens and Q_{cpp} becomes more significant. For high thermal conductivities of particles, Q_{cpp} becomes dominant, but Q_{cpfp} is still important.

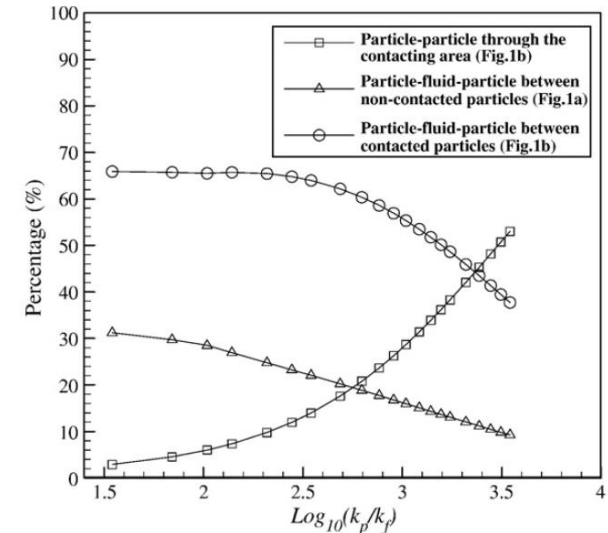


Fig. 8. Relative contributions of the heat transfer mechanisms to the overall heat transfer under the base condition (note: the percentage is the ratio of each heat flux to the total heat flux under the thermal equilibrium condition).

It was also observed that the relative importance of each conduction mechanism to the total conduction heat transfer is insensitive to the bed temperature, for low or high thermal conductivity of particles (although the total conduction contribution decreases in high temperature, as radiation contribution increases).

Heat Conduction Mechanisms

Similarly, according to Cheng et al (1999) the contribution of each conduction mechanism to the total conduction heat transfer in packed beds with a stagnant fluid, is observed as:

- **Non-contact particle-fluid-particle** (line 1):
Contribution is relatively low for most values of the ratio between particle and fluid thermal conductivities (referred to as $k_{pf} = k_p/k_f$).
- **Contact particle-fluid-particle** (line 2):
Dominant when k_{pf} is low.
- **Contact particle-particle** (line 3):
Becomes important when k_{pf} increases.

It was also shown that the relative importance of different conduction mechanisms may vary for different packing structures, so these conclusions may be affected by the particle size distribution, shapes, etc. (e.g. ellipsoids are analyzed in Gan et al, 2016).

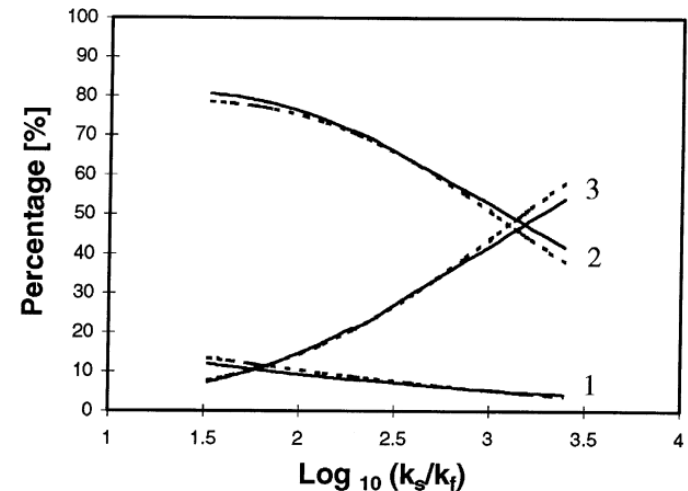


Fig. 11. Relative contributions of the heat transfer mechanisms to the overall heat transfer: line 1, the conduction through the solid particles and stagnant fluid between non-contacted particles; line 2, the conduction through the solid particles and stagnant fluid between contacted particles; and line 3, the conduction through the contact area between contacted particles; (—), Model A; (- - -), Model B ($c = 0.5$).

Heat Conduction Mechanisms

Two model types are identified for heat transfer due to direct conduction (contact particle-particle):

Collisional contact conduction

Applicable to systems in which particles are moving and colliding against each other or against walls, i.e. contacts last for a very short time (e.g. moving and fluidized beds, etc).

Static contact conduction

Applicable to systems in which particles are in static contact, i.e. there is a permanent contact and they keep in touch with no relative velocity (e.g. fixed / packed beds, granulators, etc).

Suggestion by Zhou et al (2009):

- **Fixed beds:** All contacts are static and only the static regime applies.
- **Fluidized beds:** Although contact conduction seems negligible, both regimes can be considered as follows:
 - Collisional contact conduction is used while the contact time is lower than the expected collision time (t_c).
 - Static contact conduction is used after the contact time becomes greater than the expected collision time (t_c).

Heat Conduction Mechanisms

Remarks from literature – Systems with static contacts

Batchelor & O'Brien (1977)

Contact particle-particle conduction dominates in packed beds when the interstitial medium is stagnant and composed of a material whose thermal conductivity is small compared to the particles ($k_p R_c / k_f R_p \gg 1$)

Wakao & Kato (1969)

Heat conduction between particles is known to be dominant in packed beds with high k_{pf} (>10)

Botterill et al (1989)

Heat conduction between particles is known to be dominant for packed beds with stagnant fluid at low temperatures ($< 450\text{K}$)

Vargas (2002)

The main heat transfer mechanism under packed and vacuum conditions is conduction through the contact surface of the particles

Chen et al (2019)

The solid contact conduction, solid-fluid-solid conduction, and radiation are considered in the thermal DEM model as the main heat transfer mechanisms in packed beds with stagnant fluid

Schlunder (1980)

Concluded that the mechanism of heat transfer at medium and long contact times is different to that at very short contact times

Molerus (1997)

If k_{pf} is high, the contact conductance between adjacent particles is the controlling process in both static and slowly moving beds of particles, in the presence of a stagnant interstitial gas

Zhou et al (2009)

In fixed beds, the conduction is dominant for high thermal conductivities of particles due to the large heat flux through the contact area

Quintana-Ruiz & Campello (2020)

Heat transfer in dry particle systems is often regarded to occur mostly through conduction

Morris et al (2015)

Particle–fluid–particle conduction is significant in systems where $k_p R_c / k_f R_p > 1$

Morris et al (2016)

The significance of particle-particle heat transfer relative to particle-fluid-particle conduction depends on $k_p R_c / k_f R_p$: when it is less than one, indirect conduction is dominant. For example, in sand the indirect conduction was observed as two orders of magnitude larger than the direct mechanism.

Heat Conduction Mechanisms

Remarks from literature – Systems with colliding particles

Sun & Chen (1988)

The collisional conduction is not a dominant mechanism in fluidized bed under typical conditions (it is negligible)

Saxena et al (1979)

Heat conduction during the collision between particles may be neglected in dilute flows

Fan & Zhu (1998)

Typically, heat transfer as a result of particle-particle and particle-wall contact is assumed negligible in gas-solids systems due to small contact area and short contact time

Li & Mason (2000), Schlunder (1982)

Heat conduction during the collision between particles must be included in dense flows, where particles are frequently in contact with their neighbors

Vargas (2002)

Contact conduction during collisions is the dominant heat transfer mechanism in dense slow flowing systems

Lu et al (2017)

In fluidized beds, the total conduction contribution is about 1/4 of the convection, thus the particle-particle conduction accounts for a very small fraction of the total heat transfer, even for high thermal conductivity values

Morris et al (2016a)

Particle-particle and particle–fluid–particle conductions can be neglected for many dilute systems because contacts are infrequent and durations are short. In moderate-to-dense particle flows, enduring contacts are frequent and conduction between particles is significant.

Moysey & Thompson (2005)

Since thermal conductivity of the solid particles is much greater than that of the stagnant interstitial medium, only heat transfer between particle contacts is considered in dense flow

Peng et al (2020)

In particulate flows with an average solid concentration > 0.2 , a large number of collisions occur concurrently, resulting in a significant amount of heat energy transferred through conduction through collisional contacts, which needs to be considered.

Collisional Contact Models

Model by Sun & Chen (1988)

Numerical and theoretical analysis of transient heat conduction due to particle collision, as a quantitative evaluation of the concepts initially presented by Soo (1967).

Elastic collisions based on [Hertz theory](#) and no thermal resistance between surfaces.

Heat conduction assumed to be similar to that between two semi-infinite media.

Small Fourier number: 1D heat flow is assumed and an analytical solution is obtained.

High Fourier number: A correction factor is employed based on numerical simulations.

The semi-infinite media assumption is inaccurate for large thermal conductivities of particles (overestimates the heat transfer when Fourier number is high).

Total thermal energy exchanged during impact:

$$U = C \frac{0.87\pi(R_c^{\max})^2 t_c^{1/2}}{(\rho_i c_i k_i)^{-1/2} + (\rho_j c_j k_j)^{-1/2}} (T_j - T_i)$$

where C is a correction factor obtained by numerical computation (provided in graphs).

The rate of heat transfer may be obtained by:

$$Q_{cpp} = U/t_c$$

Collisional Contact Models

Model by Zhou et al (2008)

FEM is employed to simulate the transient heat conduction between colliding spheres, assuming elastic collisions based on [Hertz theory](#).

Improved the equation of Sun & Chen (1988) to fit the FEM results.

Small Fourier number: the new equation is consistent with the analytical results of the semi-infinite media assumption of Sun & Chen (1988).

High Fourier number: the new equation solves the overestimation issue of the semi-infinite media assumption (besides not depending on a non-practical factor).

The new equation still overestimates the heat flux when the particle conductivities are significantly different, and it is not recommended for temperature dependent properties.

$$\text{Rate of heat transfer: } Q_{cpp} = C \frac{\pi(R_c^{\max})^2 t_c^{-1/2}}{(\rho_i c_i k_i)^{-1/2} + (\rho_j c_j k_j)^{-1/2}} (T_j - T_i)$$

Collisional Contact Models

Model by Zhou et al (2008)

In the previous equation:

$$C = 0.435 \left(\sqrt{C_2^2 - 4C_1(C_3 - F_o)} - C_2 \right) / C_1$$

$$C_1 = -2.300(\rho_i c_i / \rho_j c_j)^2 + 8.909(\rho_i c_i / \rho_j c_j) - 4.235$$

$$C_2 = +8.169(\rho_i c_i / \rho_j c_j)^2 - 33.770(\rho_i c_i / \rho_j c_j) + 24.885$$

$$C_3 = -5.758(\rho_i c_i / \rho_j c_j)^2 + 24.464(\rho_i c_i / \rho_j c_j) - 20.511$$

Fourier number:
$$F_o = \frac{\alpha_i t_c}{l_i^2} = \frac{k_i t_c}{\rho_i c_i (R_c^{\max})^2}$$

Static Contact Models

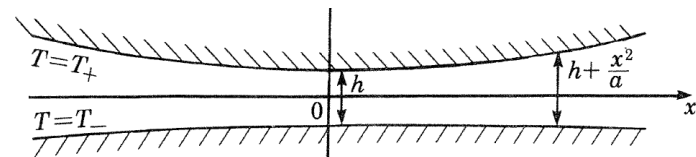
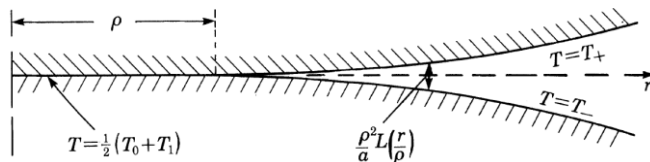
Model by Batchelor & O'Brien (1977)

Investigated thermal conduction through a homogeneous & isotropic packed granular material of round particles immersed in a uniform stagnant fluid considering:

- Stationary condition.
- Steady-state heat transfer.
- Particles with a much larger conductivity than the fluid ($k_{pf} \gg 1$):
Allows the assumption of uniform temperature distribution within particles (far from contact points), due to the relatively small temperature gradient.

Included direct and indirect conduction by analyzing two cases of particle interaction:

- Particles in contact through a flat circular area with radius R_c^{htz} .
- Particles nearly in contact with surfaces separated by a gap d_s .



Static Contact Models

Model by Batchelor & O'Brien (1977) – Particles in contact

Two smooth-elastic particles pressed together by a static compression load F_n forming a flat circle of contact whose radius is related to load following [Hertz theory](#).

2 conduction paths: directly via contact area and indirectly via annular fluid cylinder.

Dimensionless parameter for the contribution of the contact path relative to the total flow:

$$\eta = \frac{k_{pf} R_c^{\text{htz}}}{2\bar{R}}$$

Total rate of heat transfer across an extended area that includes the contact circle:

$$Q_c = 2\pi\bar{R}k_f(\tilde{H}_c + \tilde{H}_f + \ln(k_{pf}^2))(T_j - T_i)$$

$$\eta \ll 1 \quad \begin{cases} \tilde{H}_c = 0.22\eta^2 \\ \tilde{H}_f = -0.05\eta^2 \end{cases}$$
$$\eta \rightarrow \infty \quad \begin{cases} \tilde{H}_c = 2\eta/\pi \\ \tilde{H}_f = -2\ln(\eta) \end{cases}$$

The formula for $\eta \ll 1$ works with good accuracy for $\eta < 1$.

The limit $\eta \rightarrow \infty$ is usually taken as $\eta > 100$ (Dai et al, 2019; Moscardini et al, 2018).

For intermediate values $1 \leq \eta \leq 100$, a linear interpolation of both formulas is used (Dai et al, 2019; Moscardini et al, 2018).

Static Contact Models

Model by Batchelor & O'Brien (1977) – Particles in contact

In the case of $\eta \rightarrow \infty$, direct conduction through the contact area is dominating, then:

$$Q_{cpp} = 2\pi\bar{R}k_f(2\eta/\pi)(T_j - T_i) = 2k_p R_c^{\text{htz}}(T_j - T_i)$$

Generalization for different properties using [effective conductivity](#) (Cheng et al, 1999) and computing the contact radius based on the [overlap geometry](#) (Musser, 2011) so the contact area is representative of any contact model (it may need a correction due to the use of a [low stiffness](#) in the simulation):

$$Q_{cpp} = 4\bar{k}R_c^{\text{geo}}(T_j - T_i)$$

This simplification, valid for high values of k_{pf} , is used by many authors in different applications to simulate direct heat conduction, from static systems (Zhou et al, 2009) to dense flows (Vargas & McCarthy, 2001; Chaudhuri et al, 2006; Amritkar et al, 2014; Lu et al, 2017; Moysey & Thompson, 2005; Musser, 2011; and many others).

Other models have been developed (Siu & Lee, 2004; Feng et al, 2008; Sridhar & Yovanovich, 1996; Lambert & Fletcher, 1997; Chan & Tien, 1973) but this one is simple and matches experimental data for conduction through packed beds reasonably well.

Static Contact Models

Model by Batchelor & O'Brien (1977) – Particles separated

Formulated for particles separated by a distance much smaller than the radii ($d_s \ll \bar{R}$).

The heat flux across the fluid layer is confined by a cylinder of radius \bar{r} ($\gg \sqrt{2\bar{R}d_s}$).

Common practice considers the above requirements of d_s and \bar{r} to be negligible.

Dimensionless parameter for quantifying temperature uniformity within particle:

$$\lambda = \frac{k_{pf}^2 d_s}{2\bar{R}}$$

Total heat flux across a circular portion of the surface area defined by \bar{r} :

$$\lambda \ll 1$$

$\lambda < 0.10$ (Moscardini et al, 2018)

$\lambda < 0.01$ (Dai et al, 2019)

Particle temperature cannot be taken as uniform near cylinder region (relatively small region as k_{pf} is still large, but finite).

$$Q_{npfp} = 2\pi\bar{R}k_f \ln(k_{pf}^2) (T_j - T_i)$$

$$\lambda \gg 1$$

$\lambda \geq 0.10$ (Moscardini et al, 2018)

$\lambda > 100$ (Dai et al, 2019).

Particle temperature is approximately uniform and material can be considered as perfectly conducting ($k_{pf} \rightarrow \infty$).

$$Q_{npfp} = 2\pi\bar{R}k_f \ln\left(1 + \frac{\bar{r}^2}{2\bar{R}d_s}\right) (T_j - T_i)$$

*Dai et al (2019): Minimum of both formulas when $0.01 \leq \lambda \leq 100$.

Static Contact Models

Model by Batchelor & O'Brien (1977) – Particles separated

Conduction cylinder radius:

Adjustable parameter that directly affects the accuracy of results and may require an initial calibration in order to match experimental or numerical results:

→ $\bar{r} = 1.00\bar{R}$ (Kanuparthi et al, 2008; Yun & Evans, 2010 – calibrated for $k_{pf} = 120$)

→ $\bar{r} = 1.42\bar{R}$ (Moscardini et al, 2018 – experimentally calibrated for $k_{pf} = 10$)

→ $\bar{r} = 2.00\bar{R}$ (Dai et al, 2019 – calibrated for the [modified BOB model](#))

Cut-off distance:

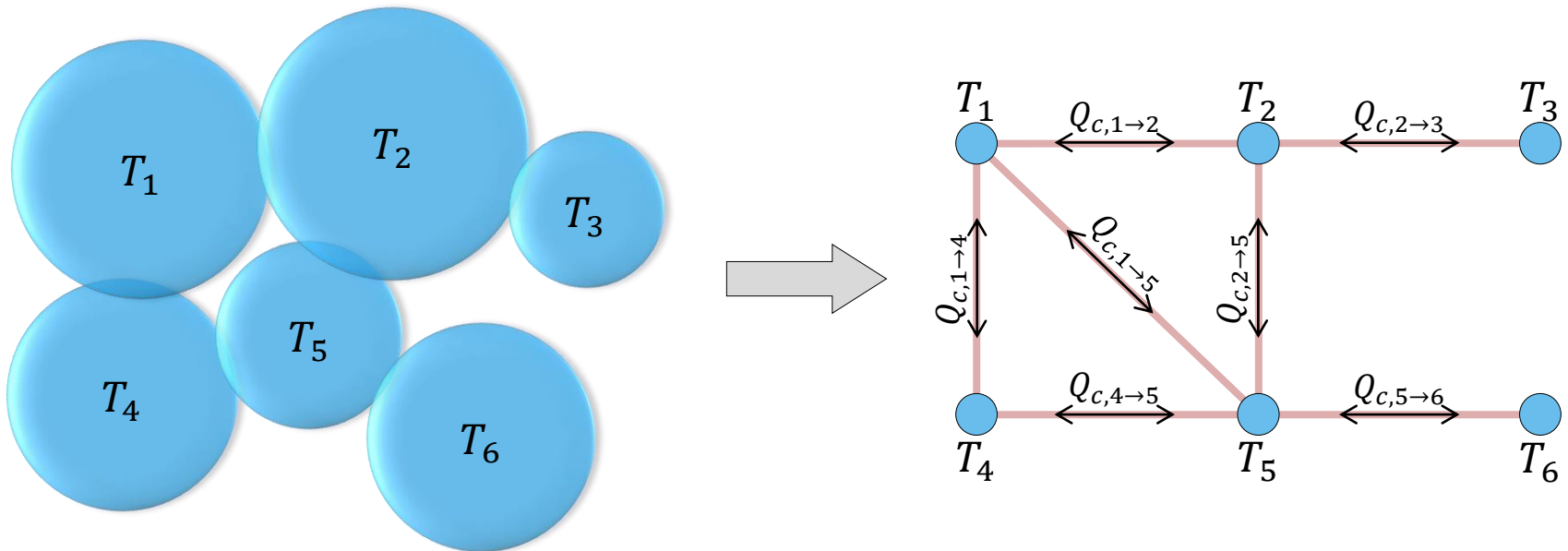
Adjustable parameter with significant effect on efficiency but small effect on accuracy, as results remain fairly constant for $d_s \geq 0.80\bar{R}$ (Yun & Evans, 2010).

It is usually taken as $d_s < 1.00\bar{R}$ (Kanuparthi et al, 2008; Yun & Evans, 2010), in order to match experimental results.

Thermal Network Models

In thermal network models, particles are viewed as nodes and their interconnections are modeled as cylinders of different radii and lengths defined by resistors to simulate the resistance to heat transfer in function of the interaction type.

Usually applied for estimating the effective conductivity of static packed systems under steady-state heat transfer condition (Moscardini et al, 2018; Dai et al, 2019), sometimes by assembling a matrix system to solve for the equilibrium temperatures of particles (Kanuparthi et al, 2008; Yun & Evans, 2010).



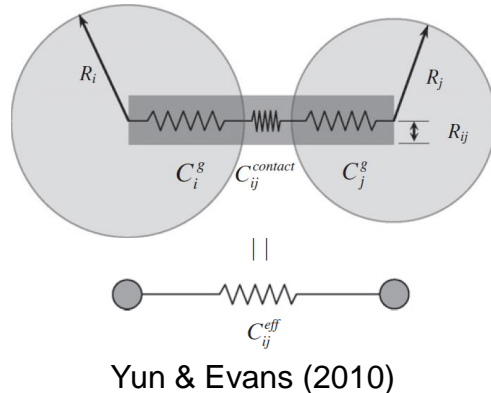
Thermal Network Models

Modified Batchelor & O'Brien model

If $k_{pf} \gg 1$ is not satisfied, the assumption of uniform temperature distribution within particles introduces an over-estimation of heat transfer.

The non-uniform temperature distribution is simplified as an equivalent temperature drop between centroid and surface, modelled as an extended cylindrical resistor.

The effective resistance is formed by a series circuit with the inner-particles resistances and the resistance of the interaction type given by the [original BOB model](#).



$$Q_c = H_{eff}(T_j - T_i)$$

$$H_{eff} = (H_i^{-1} + H_j^{-1} + H_{BOB}^{-1})^{-1}$$

$$H_i = k_i \pi \bar{r}^2 / R_i \quad H_j = k_j \pi \bar{r}^2 / R_j$$

H_{BOB} : Inter-surfaces conductance
estimated with BOB model

Dai et al (2019) proposed a correlation based on FEM that presents decent agreement with numerical results and is useful for predicting purposes when $k_{pf} < 10^3$:

$$\bar{r} = 1.3121 k_{pf}^{-0.19} \min(R_i, R_j)$$

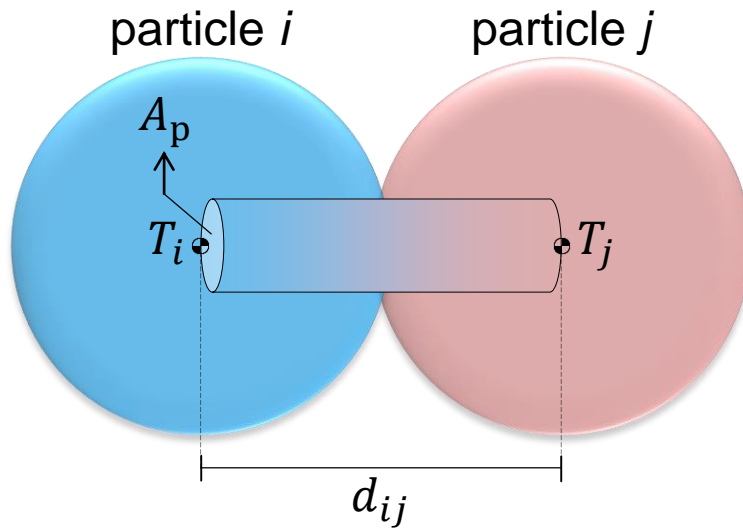
Thermal Network Models

Thermal pipe model

Heat is exchanged through a thermal pipe connecting the center of touching particles, which behave like heat reservoir (due to the lumped capacitance assumption).

Assumes the discrete form of Fourier law for the heat transfer, and the thermal resistance of the pipe may be considered in different ways.

Suited for modeling continuous materials (Jebahi et al, 2015; Hahn et al, 2011).



$$Q_{cpp} = \frac{kA_p}{d_{ij}} (T_j - T_i)$$

Thermal Network Models

Thermal pipe model by Quintana-Ruiz & Campello (2020)

Simple model for quantifying the contact heat flow under static and dynamic behavior.

$$Q_{cpp} = \frac{\tilde{k}A_p}{d_{ij}}(T_j - T_i) \quad \text{where} \quad \tilde{k} = (R_i + R_j) \left(\frac{R_i}{k_i} + \frac{R_j}{k_j} \right)^{-1} \quad A_p = \pi(R_c^{\text{geo}})^2$$

Thermal pipe model by Rojek (2014)

DEM is used for rock modeling, but as a discretization method and not to represent separate particles that come into contact.

$$Q_{cpp} = \frac{k_p A_p}{d_{ij}}(T_j - T_i) \xrightarrow{\substack{A_p = 2\tilde{r}b \\ d_{ij} = 2\tilde{r}}} Q_{pp} = k_p b(T_j - T_i)$$

2D model: b is assumed as unity.

3D model: b is assumed as \tilde{r} .

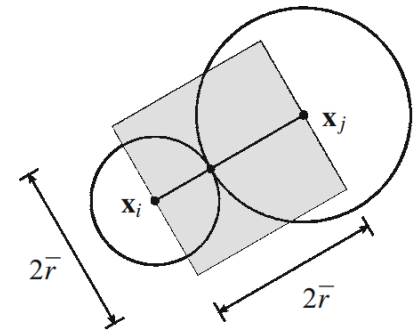


Fig. 10 Equivalence of two particles to a bar in a heat conduction problem

$$\tilde{r} = \frac{R_i + R_j}{2}$$

Voronoi-Based Models

Introduced by Cheng et al (1999), with sub-models A and B, for a packed bed with mono-sized particles in the presence of a stagnant fluid. Later modified by Gan et al (2016) and Chen et al (2019) for multi-sized particles.

May require a Voronoi tessellation (Voronoi, 1908) at each time step: time consuming.

Heat transfer between two neighboring particles is restricted to the region delineated by the double pyramid that share a Voronoi boundary plane (including particles' body).

To get an analytical solution, the double pyramid is replaced by a double tapered cone of the same area A_n (of radius r_{ij}) and distance between vertexes (particles centers).

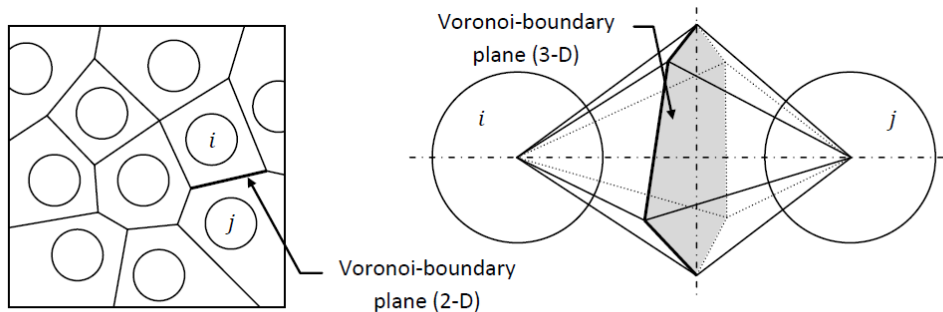
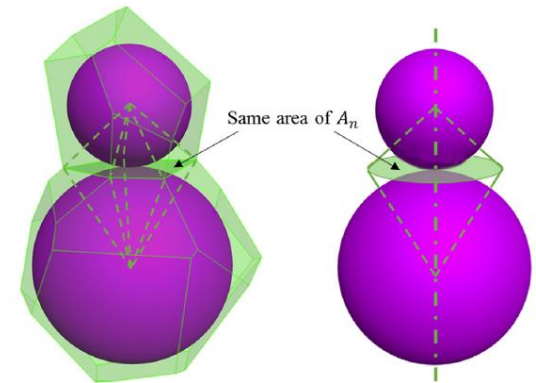


Figure 3-11: The model of Cheng, Yu, and Zulli [65] restricts particle-fluid-particle conduction to the region delineated by the double pyramid (3-D) generated by the Voronoi-boundary plane.

Musser (2011)



Chen et al (2019)

Voronoi-Based Models

Voronoi model A

- The surface of the double tapered cone is isothermal.
- Conduction is negligible in the outer region of the cone (region “B”).
- The heat flow paths are parallel to the axis joining the particles’ centers.

These assumptions lead to an integral expression for the rate of heat transfer, which needs to be solved numerically by a quadrature.

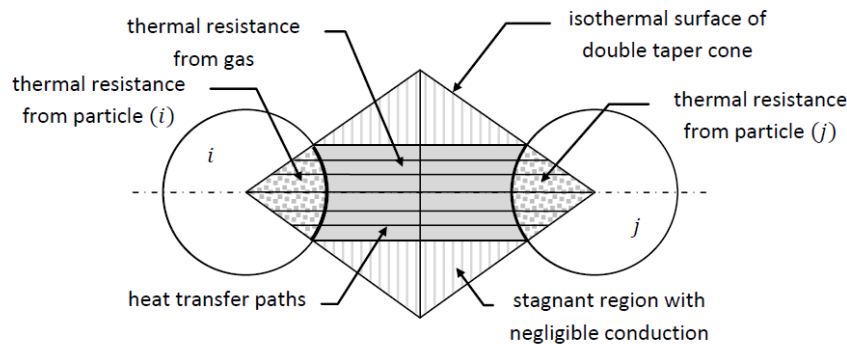
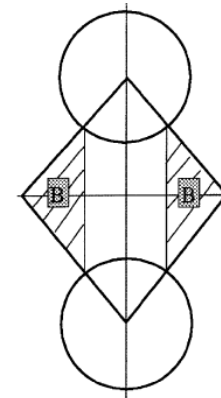


Figure 3-12: Cheng, Yu, and Zulli's [65] *Model A* for particle-fluid-particle conduction assumes that the surface of the double tapered cone is isothermal, conduction is negligible in the outer region of the double tapered cone, and the heat transfer paths are parallel to the axis joining the particles' centers.

Musser (2011)



(b) A double taper cone model with shaded area as region B

Cheng et al (1999)

Voronoi-Based Models

Voronoi model A (mono-size)

For mono-sized particles of radius R_p , Cheng et al (1999) determined that the particle-fluid-particle heat transfer rate by conduction can be obtained from:

$$Q_{pfp} = (T_j - T_i) \int_{R_c}^{r_{sf}} \frac{2\pi r}{\frac{1}{k} \left(\sqrt{R_p^2 - r^2} - \frac{d_{ij}r}{2r_{ij}} \right) + \frac{1}{k_f} \left(d_{ij} - 2\sqrt{R_p^2 - r^2} \right)} dr$$

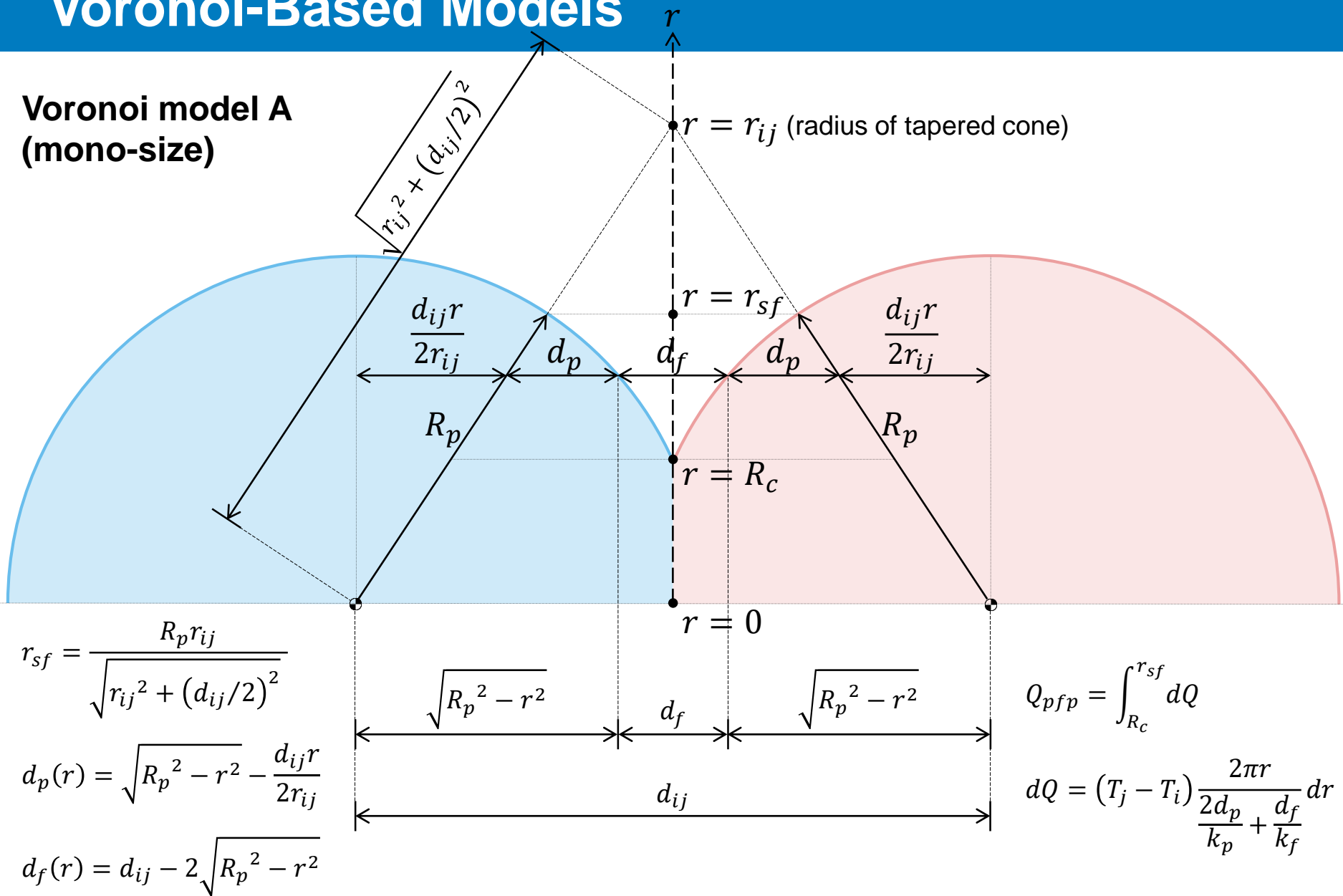
where: $r_{ij} = \sqrt{\frac{3V_{ij}}{\pi d_{ij}}}$ $r_{sf} = \frac{R_p r_{ij}}{\sqrt{r_{ij}^2 + (d_{ij}/2)^2}}$

V_{ij} is the volume of the Voronoi polyhedron (i.e. the double tapered cone) between particles, which is actually the only parameter that depends on the Voronoi tessellation.

When particles are not in contact, $R_c = 0$.

Voronoi-Based Models

Voronoi model A (mono-size)



Voronoi-Based Models

Voronoi model A (multiple-sizes)

For multi-sized particles, Norouzi et al (2016) suggested applying the same formula by simply using the average radius:

$$R_p = \frac{R_i + R_j}{2}$$

Gan et al (2016), on the other hand, extended this model for ellipsoids with different sizes (however, a validation for multi-sized spheres has not been reported).

$$Q_{pfp} = (T_j - T_i) \int_{R_c}^{r_{sf}} \frac{2\pi r}{\frac{1}{k_i} \left(\beta_i - \frac{D_i r}{r_{ij}} \right) + \frac{1}{k_j} \left(\beta_j - \frac{D_j r}{r_{ij}'} \right) + \left(\frac{d_{ij} - \beta_i - \beta_j}{k_f} \right)} dr$$

$$\beta_i = \sqrt{R_i^2 - r^2} \quad \beta_j = \sqrt{R_j^2 - r^2}$$

When particles are not in contact, $R_c = 0$.

Voronoi-Based Models

Voronoi model A (multiple-sizes)

$$D_i = \begin{cases} \frac{R_i^2 - R_j^2 + d_{ij}^2}{2d_{ij}} & \text{if particles are not in contact} \\ \sqrt{R_i^2 - R_c^2} & \text{if particles are in contact} \end{cases}$$

$$D_j = d_{ij} - D_i$$

$$r_{sf} = \begin{cases} \frac{R_i r_{ij}}{\sqrt{r_{ij}^2 + D_i^2}} & \text{if } R_i \leq R_j \\ \frac{R_j r_{ij}}{\sqrt{r_{ij}^2 + D_j^2}} & \text{if } R_i > R_j \end{cases}$$

Since r_{sf} is calculated based on the smaller particle, it might underestimate the heat transfer when particles have very different sizes (Peng et al, 2020).

$$r_{ij}' = \frac{D_j r_{sf}}{\sqrt{R_j^2 - r_{sf}^2}}$$

Voronoi-Based Models

Voronoi model B

- Each particle has an isothermal core of radius r_c , with the particle representative temperature.
- Heat transfer paths radiate from the cores' surfaces.

These assumptions lead to an expression that, although it does not need to solve an integral numerically, relies on an input fitting parameter (the radius of isothermal core).

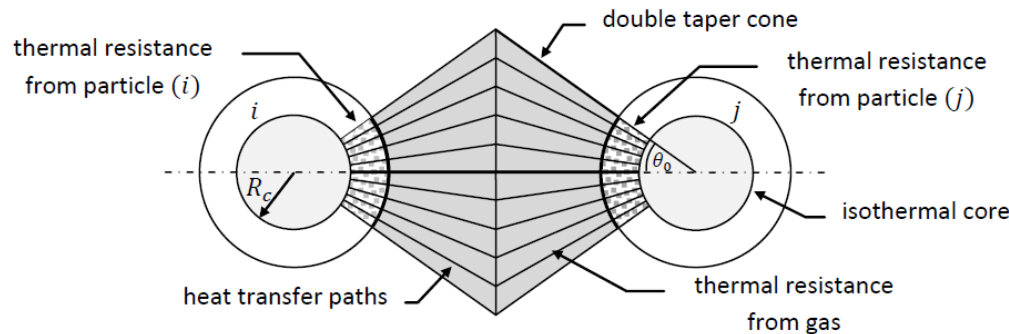
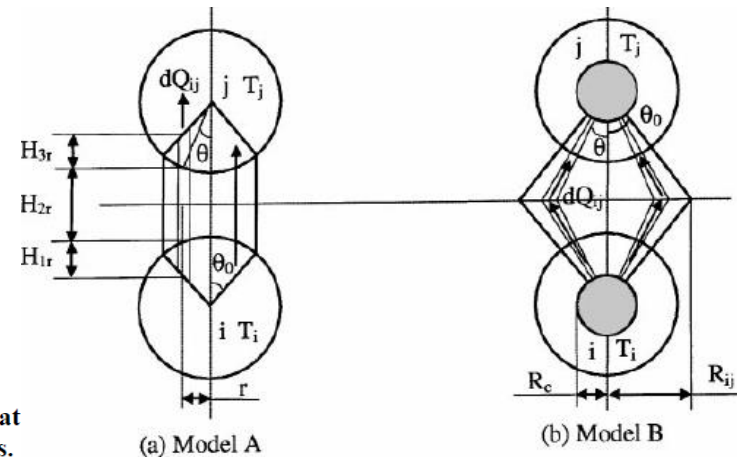


Figure 3-14: Cheng, Yu, and Zulli's [65] *Model B* for particle-fluid-particle conduction assumes that each particle has an isothermal core and the paths of heat transfer radiate from the particles centers.

Musser (2011)



Cheng et al (1999)

Voronoi-Based Models

Voronoi model B

The value of the isothermal core radius affects the results specially when k_{pf} is not very high (< 1000), since a high ratio indicates that the resistance to heat conduction within particles is negligible.

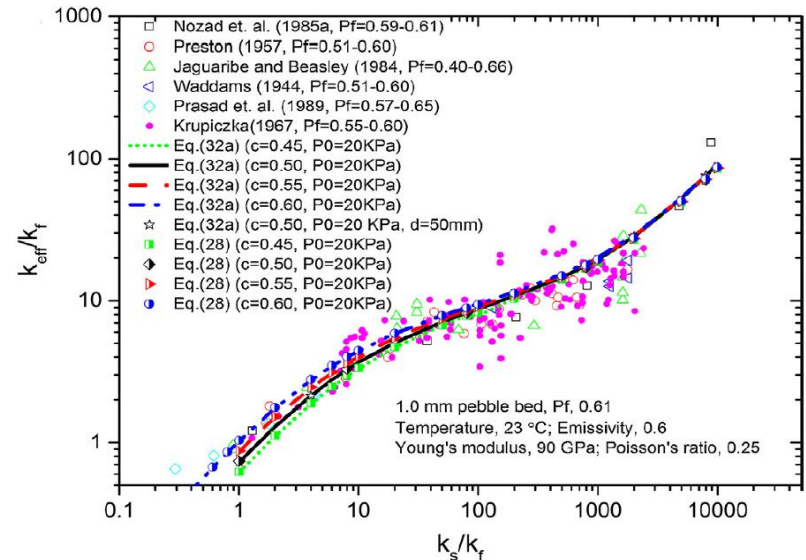
For mono-sized particles, Cheng et al (1999) observed that $r_c = 0.5R_p$ provides results that are in good agreement with Voronoi model A.

For multiple-sized particles, Chen et al (2019) compared the numerical results with experimental data and suggested:

$$r_c = 0.5R_p \quad \text{if} \quad 5 < k_p/k_f < 10^4$$

$$r_c = 0.6R_p \quad \text{if} \quad 1 < k_p/k_f < 5$$

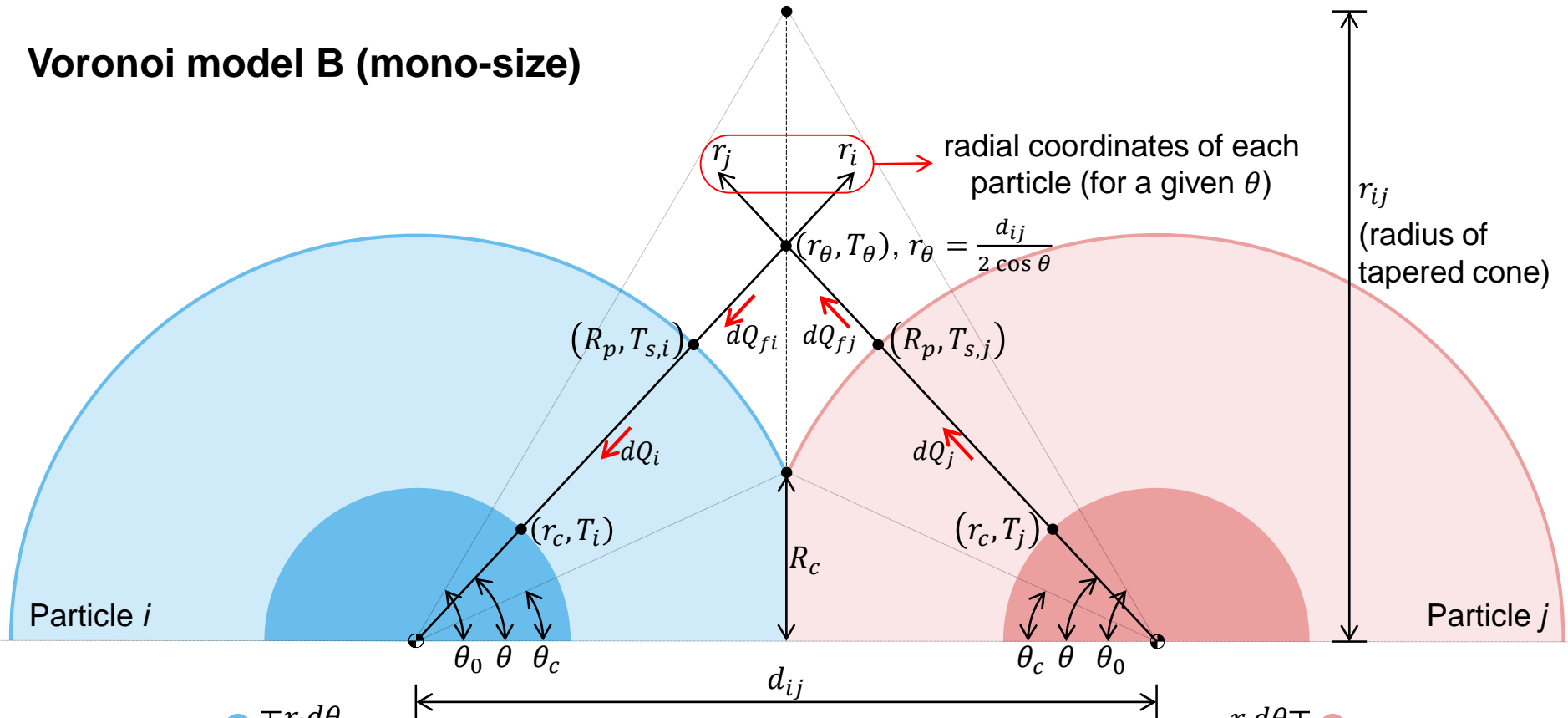
For $k_p/k_f < 1$, the isothermal core assumption no longer holds and model B is not valid.



Chen et al (2019)

Voronoi-Based Models

Voronoi model B (mono-size)



4 paths of heat flow from particle j to i :

- 1) Inside particle j (dQ_j): from $r_j = r_c$ to $r_j = R_p$
- 2a) Through fluid (dQ_{fj}): from $r_j = R_p$ to $r_j = r_\theta$
- 2b) Through fluid (dQ_{fi}): from $r_i = r_\theta$ to $r_i = R_p$
- 3) Inside particle i (dQ_i): from $r_i = R_p$ to $r_i = r_c$

Voronoi-Based Models

Voronoi model B (mono-size)

$$dQ_j = (r_j d\theta \cdot 2\pi r_j \sin \theta)(-k_j dT/dr_j) = -2\pi k_j r_j^2 \sin \theta d\theta dT/dr_j \rightarrow dT = -\frac{dQ_j}{2\pi k_j \sin \theta d\theta} \frac{dr_j}{r_j^2}$$

$$\left. \begin{array}{l} r_j = r_c \rightarrow T = T_j \\ r_j = R_p \rightarrow T = T_{s,j} \end{array} \right\} \int_{T_j}^{T_{s,j}} dT = \int_{r_c}^{R_p} -\frac{dQ_j}{2\pi k_j \sin \theta d\theta} \frac{dr_j}{r_j^2} \rightarrow T_j - T_{s,j} = \frac{dQ_j}{2\pi k_j \sin \theta d\theta} \left(\frac{1}{r_c} - \frac{1}{R_p} \right)$$

$$dQ_{fj} = (r_j d\theta \cdot 2\pi r_j \sin \theta)(-k_f dT/dr_j) = -2\pi k_f r_j^2 \sin \theta d\theta dT/dr_j \rightarrow dT = -\frac{dQ_{fj}}{2\pi k_f \sin \theta d\theta} \frac{dr_j}{r_j^2}$$

$$\left. \begin{array}{l} r_j = R_p \rightarrow T = T_{s,j} \\ r_j = r_\theta \rightarrow T = T_\theta \end{array} \right\} \int_{T_{s,j}}^{T_\theta} dT = \int_{R_p}^{r_\theta} -\frac{dQ_{fj}}{2\pi k_f \sin \theta d\theta} \frac{dr_j}{r_j^2} \rightarrow T_{s,j} - T_\theta = \frac{dQ_{fj}}{2\pi k_f \sin \theta d\theta} \left(\frac{1}{R_p} - \frac{1}{r_\theta} \right)$$

$$dQ_{fi} = (r_i d\theta \cdot 2\pi r_i \sin \theta)(k_f dT/dr_i) = 2\pi k_f r_i^2 \sin \theta d\theta dT/dr_i \rightarrow dT = \frac{dQ_{fi}}{2\pi k_f \sin \theta d\theta} \frac{dr_i}{r_i^2}$$

$$\left. \begin{array}{l} r_i = r_\theta \rightarrow T = T_\theta \\ r_i = R_p \rightarrow T = T_{s,i} \end{array} \right\} \int_{T_\theta}^{T_{s,i}} dT = \int_{r_\theta}^{R_p} \frac{dQ_{fi}}{2\pi k_f \sin \theta d\theta} \frac{dr_i}{r_i^2} \rightarrow T_\theta - T_{s,i} = \frac{dQ_{fi}}{2\pi k_f \sin \theta d\theta} \left(\frac{1}{R_p} - \frac{1}{r_\theta} \right)$$

$$dQ_i = (r_i d\theta \cdot 2\pi r_i \sin \theta)(k_i dT/dr_i) = 2\pi k_i r_i^2 \sin \theta d\theta dT/dr_i \rightarrow dT = \frac{dQ_i}{2\pi k_i \sin \theta d\theta} \frac{dr_i}{r_i^2}$$

$$\left. \begin{array}{l} r_i = R_p \rightarrow T = T_{s,i} \\ r_i = r_c \rightarrow T = T_i \end{array} \right\} \int_{T_{s,i}}^{T_i} dT = \int_{R_p}^{r_c} \frac{dQ_i}{2\pi k_i \sin \theta d\theta} \frac{dr_i}{r_i^2} \rightarrow T_{s,i} - T_i = \frac{dQ_i}{2\pi k_i \sin \theta d\theta} \left(\frac{1}{r_c} - \frac{1}{R_p} \right)$$

Voronoi-Based Models

Voronoi model B (mono-size)

Adding the resulting highlighted equations and rearranging the terms (the terms $dQ_i = dQ_j = dQ_{fi} = dQ_{fj}$ are expressed simply as dQ):

$$dQ = \frac{T_j - T_i}{\frac{1/r_c - 1/R_p}{2\pi k_i \sin \theta} + \frac{1/r_c - 1/R_p}{2\pi k_j \sin \theta} + \frac{1/R_p - 1/r_\theta}{\pi k_f \sin \theta}} d\theta = (T_j - T_i)\pi \frac{\sin \theta}{a - b \cos \theta} d\theta$$

Where:
$$a = \frac{1}{2\bar{k}} \left(\frac{1}{r_c} - \frac{1}{R_p} \right) + \frac{1}{k_f R_p} \quad b = \frac{2}{k_f d_{ij}}$$

The total heat transfer rate is obtained by integrating the elementary heat rate over the range of angles that define the tapered cone:

$$Q_{pfp} = \int_{\theta_c}^{\theta_0} dQ = (T_j - T_i)\pi \int_{\theta_c}^{\theta_0} \frac{\sin \theta}{a - b \cos \theta} d\theta$$

Voronoi-Based Models

Voronoi model B (mono-size)

Cheng et al (1999) performed this integration and determined that the particle-fluid-particle heat transfer rate by conduction can be expressed as:

$$Q_{pfp} = (T_j - T_i) \frac{\pi}{b} \ln \left(\frac{a - b \cos \theta_0}{a - b \cos \theta_c} \right)$$

$$a = \frac{1}{2\bar{k}} \left(\frac{1}{r_c} - \frac{1}{R_p} \right) + \frac{1}{k_f R_p}$$

$$\cos \theta_0 = \frac{d_{ij}}{2\sqrt{r_{ij}^2 + (d_{ij}/2)^2}}$$

$$b = \frac{2}{k_f d_{ij}}$$

$$\cos \theta_c = \frac{d_{ij}}{2\sqrt{R_c^2 + (d_{ij}/2)^2}}$$

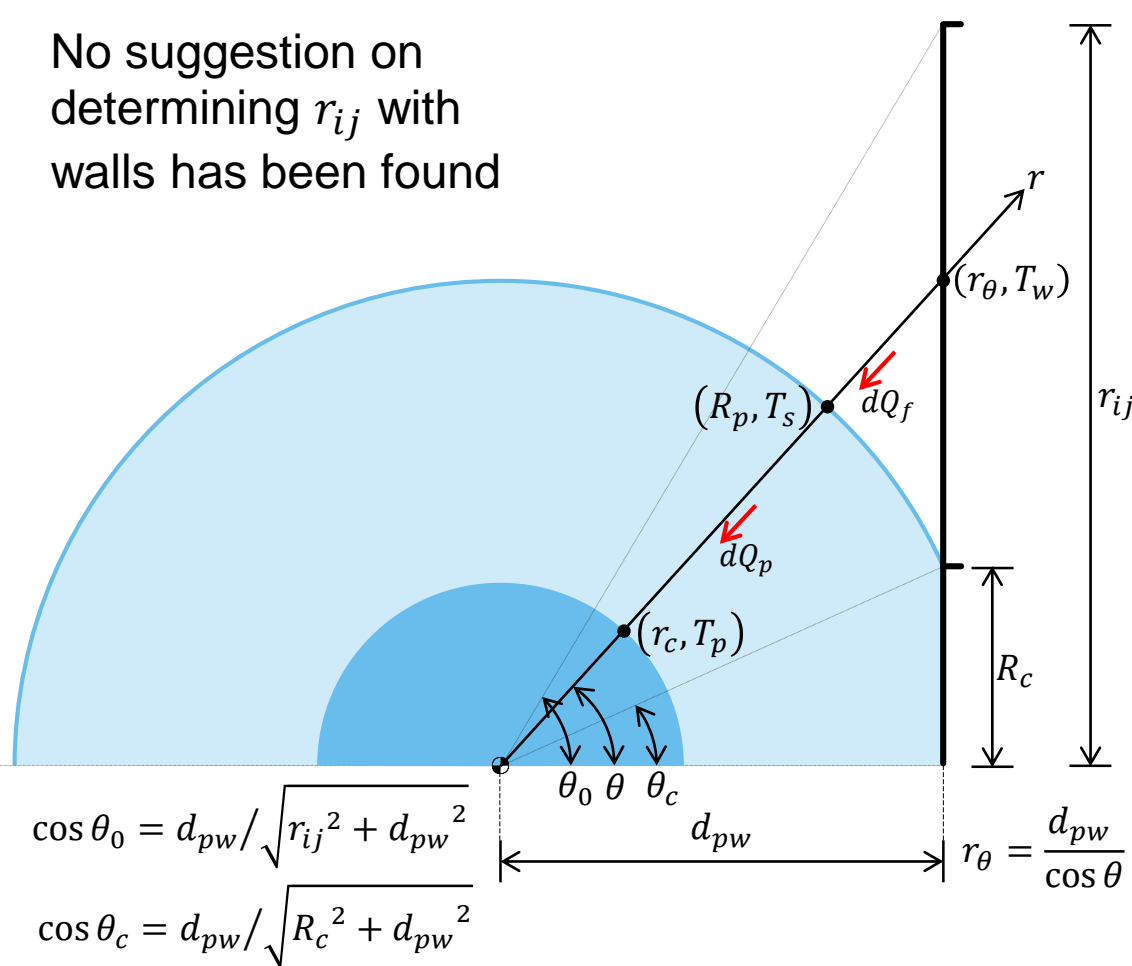
When particles are not in contact, $R_c = 0$.

Voronoi-Based Models

Voronoi model B (interaction with walls)

Interaction with flat walls can be similarly addressed by adapting the geometry:

No suggestion on determining r_{ij} with walls has been found



$$dQ_f = 2\pi k_f r^2 \sin \theta d\theta dT/dr$$

$$dQ_p = 2\pi k_p r^2 \sin \theta d\theta dT/dr$$

$$T_w - T_s = \frac{dQ_f}{2\pi k_f \sin \theta d\theta} \left(\frac{1}{R_p} - \frac{1}{r_\theta} \right)$$

$$T_s - T_p = \frac{dQ_p}{2\pi k_p \sin \theta d\theta} \left(\frac{1}{r_c} - \frac{1}{R_p} \right)$$

$$dQ = \frac{T_w - T_p}{\frac{1/r_c - 1/R_p}{2\pi k_p \sin \theta} + \frac{1/R_p - 1/r_\theta}{2\pi k_f \sin \theta}} d\theta$$

$$Q_{pfw} = (T_w - T_p) \frac{\pi}{b} \ln \left(\frac{a - b \cos \theta_0}{a - b \cos \theta_c} \right)$$

$$a = \frac{1}{2k_p} \left(\frac{1}{r_c} - \frac{1}{R_p} \right) + \frac{1}{2k_f R_p} \quad b = \frac{1}{2k_f d_{pw}}$$

Voronoi-Based Models

Voronoi model B (multiple-sizes)

For multi-sized particles, Chen et al (2019) improved the model:

$$\Lambda > 0 \quad \rightarrow \quad Q_{pfp} = (T_j - T_i) \frac{\pi k_f d_{ij} (1 - \Delta\gamma^2)}{2\sqrt{|\Lambda|}} \ln \left| \frac{1 - Y_1}{1 + Y_1} \right|$$

$$\Lambda = 0 \quad \rightarrow \quad Q_{pfp} = (T_j - T_i) \frac{\pi k_f d_{ij} (1 - \Delta\gamma^2)}{A + B} \left(\frac{1}{\delta_i^{\min}} - \frac{1}{\delta_i^{\max}} \right)$$

$$\Lambda < 0 \quad \rightarrow \quad Q_{pfp} = (T_j - T_i) \frac{\pi k_f d_{ij} (1 - \Delta\gamma^2)}{2\sqrt{|\Lambda|}} \tan^{-1}(Y_2)$$

$$\text{where: } \begin{cases} \Lambda = (1 + \Delta\gamma A)(1 - \Delta\gamma B) \\ \Delta\gamma = \gamma_j - \gamma_i \quad \begin{cases} \gamma_i = R_i/d_{ij} \\ \gamma_j = R_j/d_{ij} \end{cases} \end{cases}$$

For mono-sized particles $\gamma_i = \gamma_j$, and this model reduces to the original one of Cheng et al (1999).

Voronoi-Based Models

Voronoi model B (multiple-sizes)

$$Y_1 = \frac{X_{\max} - X_{\min}}{1 - X_{\max}X_{\min}}$$

$$Y_2 = \frac{X_{\max} - X_{\min}}{1 + X_{\max}X_{\min}}$$

$$X_{\max} = \frac{(A + B)\delta_i^{\max} + \Delta\gamma B - 1}{\sqrt{|\Lambda|}}$$

$$X_{\min} = \frac{(A + B)\delta_i^{\min} + \Delta\gamma B - 1}{\sqrt{|\Lambda|}}$$

$$A = \frac{k_i + k_f(R_i/r_{c,i} - 1)}{k_i\gamma_i}$$

$$B = \frac{k_j + k_f(R_j/r_{c,j} - 1)}{k_j\gamma_j}$$

$$\delta_i^{\max} = \frac{1}{2} \left(\sqrt{1 + \frac{4A_n}{\pi d_{ij}^2 (1 - \Delta\gamma^2)}} - \Delta\gamma \right)$$

$$\delta_i^{\min} = \frac{1}{2} \left(\sqrt{1 + \frac{4R_c^2}{d_{ij}^2 (1 - \Delta\gamma^2)}} - \Delta\gamma \right)$$

A_n is the nominal area for the neighboring Voronoi cells.

When particles are not in contact, $R_c = 0$.

Voronoi-Based Models

Remarks

When particles are moving, it is computationally demanding to build the transient Voronoi polyhedra at every time step.

However, the only parameters of the previous models that depend on the shape of the polyhedra are the volume V_{ij} , to compute the radius r_{ij} , and the area A_n .

Yang et al (2002) established a relationship between the average face area of the Voronoi polyhedra and the packing density of mono-sized fine particles.

Zhou et al (2009) used these results to compute the mentioned parameters from the local porosity ε_i (i.e. local void fraction) around particle i , which is usually an output of DEM simulations so that the Voronoi tessellation would not be needed:

$$A_n = 0.985R_i^2(1 - \varepsilon_i)^{-2/3} \qquad r_{ij} = \sqrt{A_n/\pi} = 0.560R_i(1 - \varepsilon_i)^{-1/3}$$

P.S. For multi-sized particles, the radius of particle i , R_i , is used to compute r_{ij} .

Voronoi-Based Models

Remarks

The particle-fluid-particle conductive heat transfer rate decreases sharply when the distance between two non-contacting particles becomes larger.

When two particles are far away from each other, although their Voronoi polyhedra are neighbors, indirect conduction should be neglected.

Using Voronoi model A with mono-sized spheres, Zhou et al (2009) suggested that indirect conduction can be ignored when the distance between the surfaces of two particles is greater than or equal to their radius ($d_{ij} \geq 3R_p$).

For the other Voronoi-based models, a similar cut-off value should be set.

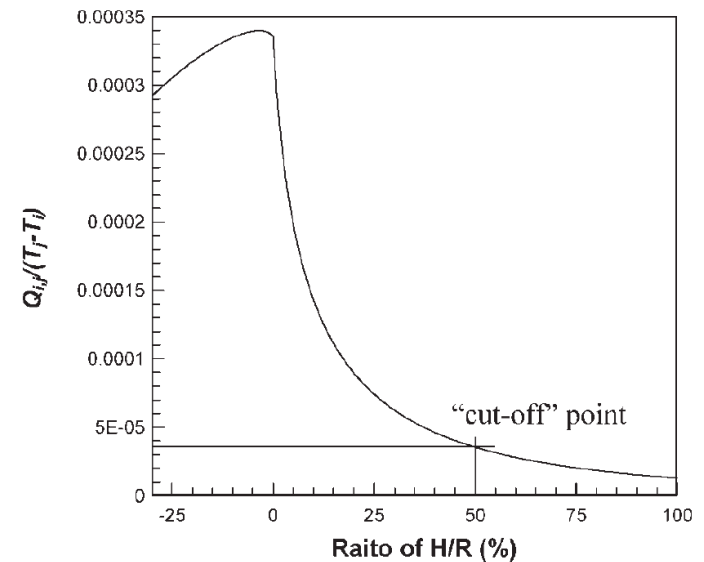


Figure 2. Variation of $Q_{i,j}/(T_j - T_i)$ with the ratio of H/R (%), calculated by Eq. 14a.

Zhou et al (2009)

Surrounding Layer Models

Introduced by Rong & Horio (1999), similarly to Delvosalle and Vanderschuren (1985), for mono-sized particles and later modified by Musser (2011) for multi-sized particles.

- Each particle is surrounded by a fluid layer of thickness δ_f , proportional to its radius.
- Heat transfer starts when the layer of a particle intersects the surface of another (i.e. $d_{ij} < R_i + R_j + \max(\delta_{f,i}, \delta_{f,j})$).
- A thin uniform fluid layer separates the particles' surfaces when they are in contact (i.e. there is a minimum separation, or conduction, distance of thickness S).
- Heat transfer paths are parallel to the axis joining the particles' centers.

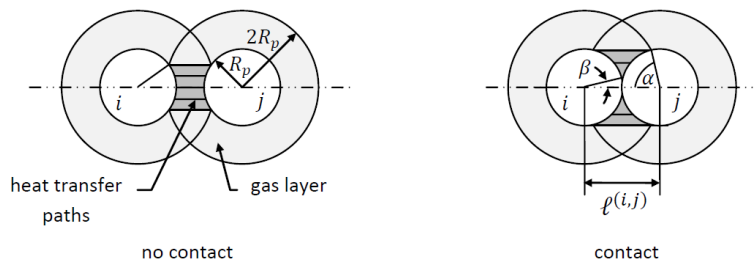
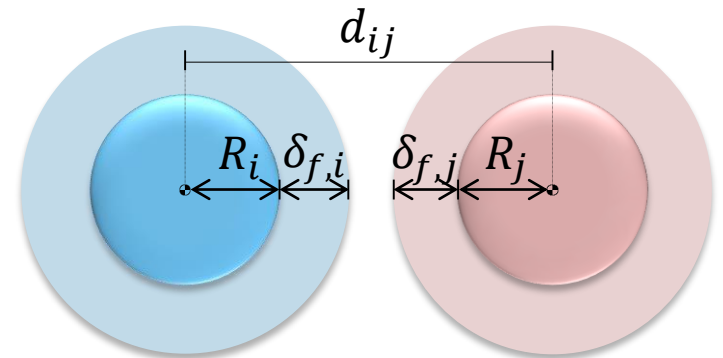


Figure 3-15: Rong and Horio's [16] configuration for particle-fluid-particle conduction. In their model, each particle is surrounded by a gas layer and heat transfer occurs across paths parallel to the line connecting the centers of the particles. When particles engage in contact, the overlap region is assumed to have a uniform gas layer separating the particles' surfaces.

Musser (2011)



The fluid layer considered as "static" due to no-slip condition over small distances and no density-driven flow (Lattanzi & Hrenya, 2017)

Surrounding Layer Models

Model by Rong & Horio (1999)

For mono-sized particles of radius R_p , the heat conduction is calculated as:

$$\begin{aligned}
 & \left. \begin{aligned}
 & 2R_p + \delta_f > d_{ij} > 2R_p \\
 & \text{(fluid layers intersecting surfaces)}
 \end{aligned} \right\} \rightarrow Q_{pfp} = (T_j - T_i)k_f \int_0^{\theta_2} \frac{2\pi R_p \sin \theta}{d_{ij} - 2R_p \cos \theta} d(R_p \sin \theta) \\
 & \left. \begin{aligned}
 & d_{ij} \leq 2R_p \\
 & \text{(Particles in contact)}
 \end{aligned} \right\} \rightarrow Q_{pfp} = (T_j - T_i)k_f \int_{\theta_1}^{\theta_2} \frac{2\pi R_p \sin \theta}{d_{ij} - 2R_p \cos \theta} d(R_p \sin \theta) \\
 & \quad + (T_j - T_i)k_f \frac{\pi(R_p \sin \theta_1)^2}{S} \rightarrow \text{Uniform conduction across the contact area, through the minimum separation distance (it is considered as the } Q_{cpp}\text{)}
 \end{aligned}$$

Where:

$$\theta_1 = \max \left(\cos^{-1} \left(\frac{d_{ij}}{2R_p} \right), \cos^{-1} \left(\frac{2R_p - S}{2R_p} \right) \right) \quad \theta_2 = \cos^{-1} \left(\frac{d_{ij}^2 + R_p^2 - (R_p + \delta_f)^2}{2R_p d_{ij}} \right)$$

Surrounding Layer Models

Model by Musser (2011)

- Discarded the contact conduction term, since it is already being considered by the appropriate models presented previously for direct heat conduction.
- Modified the geometry to consider multi-sized particles.
- Changed variables to allow the integral to be solved by basic quadrature routines.

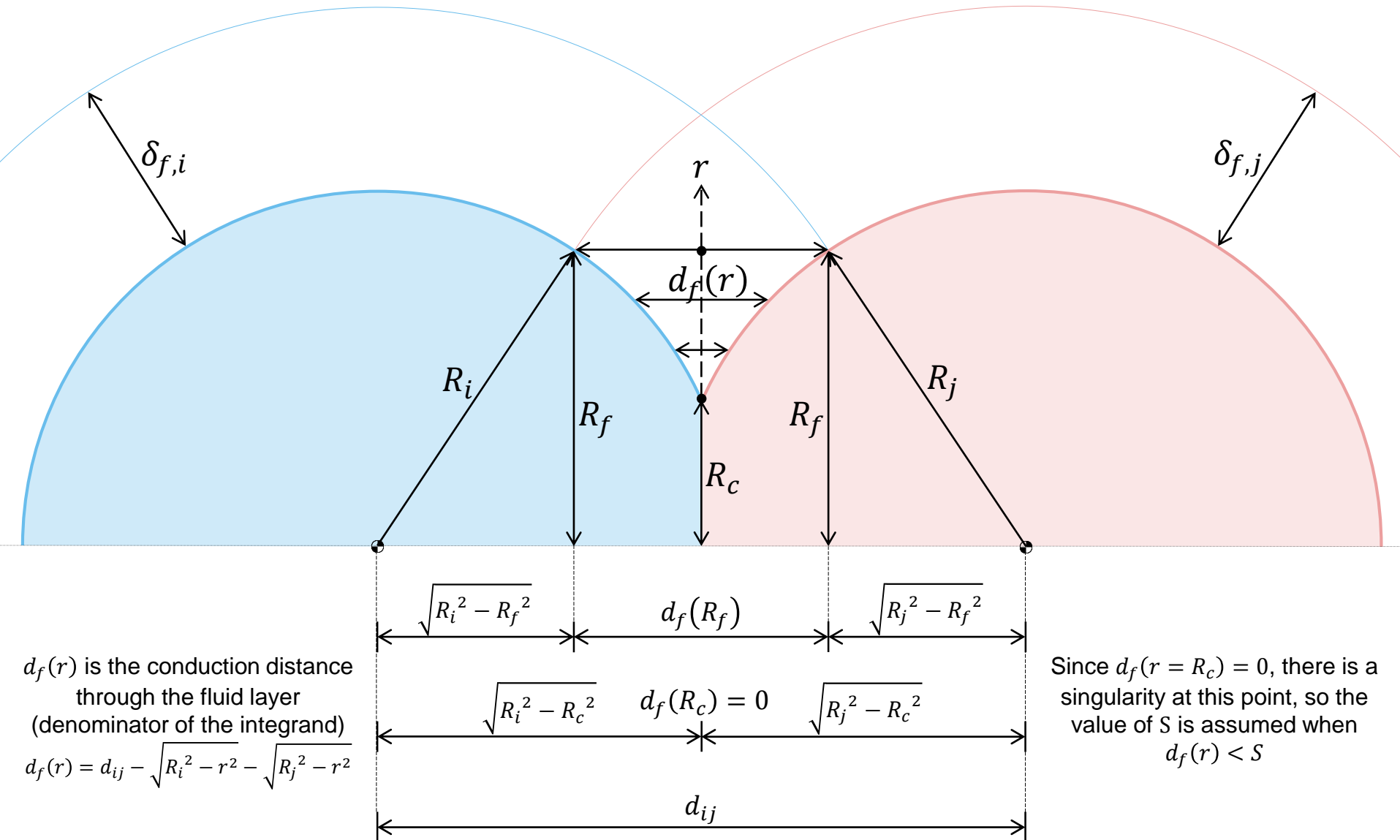
$$Q_{pfp} = (T_j - T_i)k_f \int_{R_c}^{R_f} \frac{2\pi r}{\max\left(S, d_{ij} - \sqrt{R_i^2 - r^2} - \sqrt{R_j^2 - r^2}\right)} dr$$

Where:

$$R_f = \sqrt{(R_k + \delta_{f,k})^2 - \left(\left((R_k + \delta_{f,k})^2 - R_l^2 + d_{ij}^2\right)/2d_{ij}\right)^2} \quad \begin{cases} R_k = \max(R_i, R_j) \\ R_l = \min(R_i, R_j) \end{cases}$$

$$R_c = \begin{cases} 0 & \text{if } d_{ij} > R_i + R_j \text{ (i.e. particles are not in contact)} \\ R_c^{\text{geo}} & \text{if } d_{ij} \leq R_i + R_j \text{ (i.e. particles are in contact)} \end{cases}$$

Surrounding Layer Models



Surrounding Layer Models

Lower integration boundary

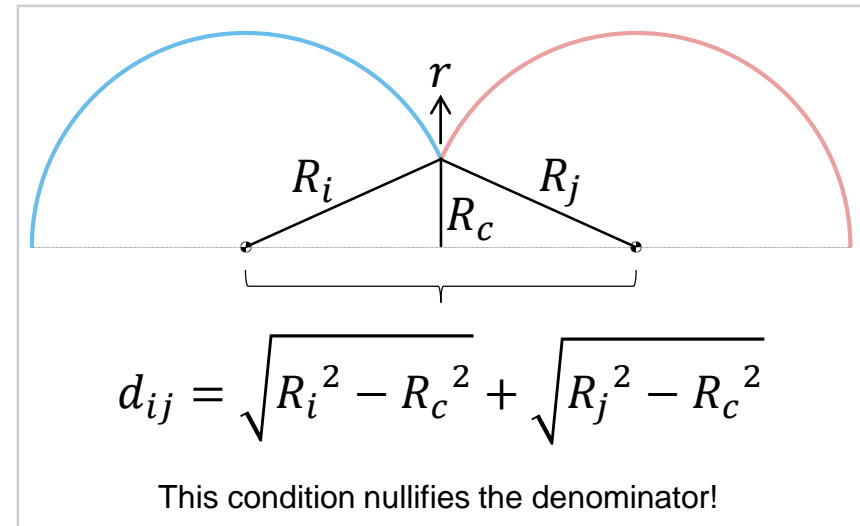
At the lower boundary R_c , the denominator becomes zero (i.e. an infinite heat flow) if the value of S is not considered as a minimum threshold value.

Mathematically, the minimum separation is needed to avoid a singularity in the integral term when particles are touching.

Physically, the minimum separation is related to the height of the surface asperities, so its value is sometimes determined by the surface roughness in non-smooth particles.

By applying the minimum separation when the denominator goes to zero, the issue is corrected by prohibiting a perfect contact between particles.

Due to the sharp variations across the integral boundary, a robust quadrature should be used for integrating (Musser, 2011, suggested an Adaptive Simpson's method).

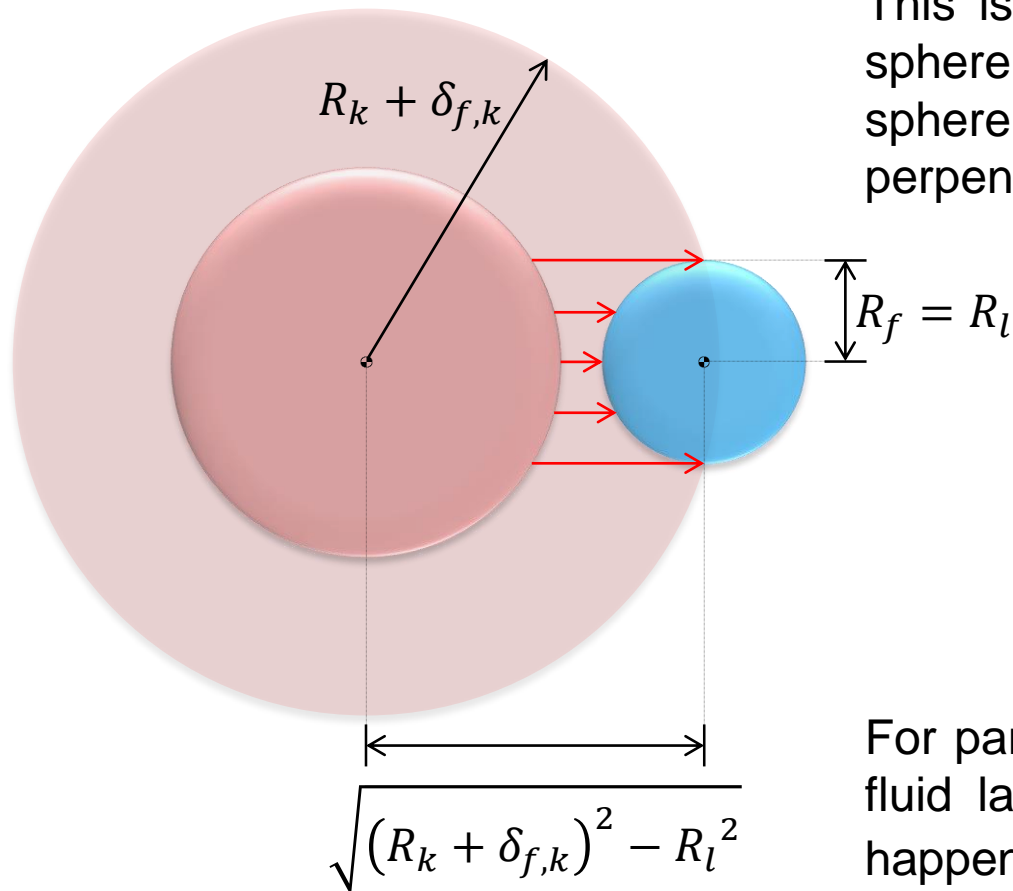


Surrounding Layer Models

Upper integration boundary

The upper boundary R_f , must be limited to the size of the radius of the smaller particle:

This is applicable when the fluid layer of one sphere intersects the surface of the other sphere in a point beyond its centerline perpendicular to the flow paths.



$$\text{If } d_{ij} \leq \sqrt{(R_k + \delta_{f,k})^2 - R_l^2}$$

$$\text{then } R_f = R_l$$

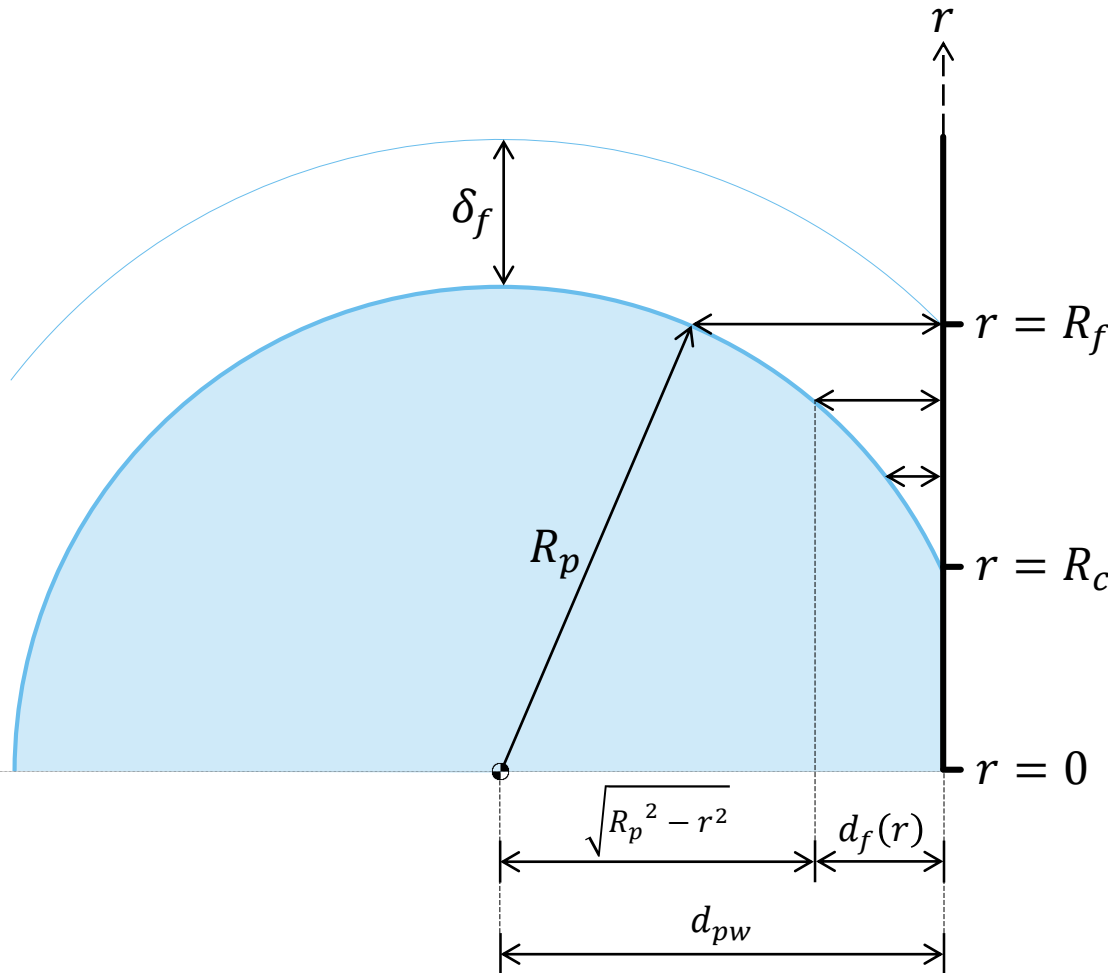
$$\text{where: } \begin{cases} R_k = \max(R_i, R_j) \\ R_l = \min(R_i, R_j) \end{cases}$$

For particles with the same size, the maximum fluid layer thickness to avoid this situation to happen is $\delta_f = (\sqrt{2} - 1)R_p \cong 0.41R_p$

Surrounding Layer Models

Interaction with walls

Interaction with flat walls can be similarly addressed by adapting the geometry:



$$Q_{pfw} = (T_w - T_p)k_f \int_{R_c}^{R_f} \frac{2\pi r}{\max(S, d_f(r))} dr$$

$$d_f(r) = d_{pw} - \sqrt{R_p^2 - r^2}$$

$$R_f = \sqrt{(R_p + \delta_f)^2 - d_{pw}^2}$$

The upper boundary, must be limited to the radius of the particle:

$$\text{If } d_{pw} \leq \sqrt{(R_p + \delta_f)^2 - R_p^2}$$

$$\text{then } R_f = R_p$$

Surrounding Layer Models

Interaction with walls

For particle-wall contacts, an analytical solution for the integral expression was given in Morris (2015), Lattanzi & Hrenya (2017) and Lu et al (2017). One way to write it is:

$$Q_{pfw} = 2\pi(T_w - T_p)k_f R_p ((a + 1) \ln(|b - a - 1|/|a - c + 1|) + b - c)$$

Where:

$$a = (d_{pw} - R_p)/R_p$$

$$b = \sqrt{1 - r_{out}^2}$$

$$c = \sqrt{1 - r_{in}^2}$$

$$r_{in} = \begin{cases} 0 & \text{if } d_{pw} > R_p + S \\ \sqrt{1 - \left(\frac{S}{R_p} - a - 1\right)^2} & \text{if } d_{pw} \leq R_p + S \end{cases}$$

$$r_{out} = \begin{cases} \sqrt{\left(\frac{R_p + \delta_f}{R_p}\right)^2 - (a + 1)^2} & \text{if } a > \sqrt{\left(\frac{R_p + \delta_f}{R_p}\right)^2 - 1} - 1 \\ 1 & \text{if } a \leq \sqrt{\left(\frac{R_p + \delta_f}{R_p}\right)^2 - 1} - 1 \end{cases}$$

Surrounding Layer Models

Input parameters

The model requires input values of two parameters for the particles: fluid layer thickness δ_f , and minimum separation distance S .

Values of δ and s used for calculating the indirect particle-fluid-particle conduction by the surrounding layer method. (Peng et al, 2020)

Author(s)	Particle size d_p (mm)	Layer thickness δ (mm)	Min. conduction distance s (m)
Rong and Horio(1999)	1	r_p	4×10^{-10}
Morris et al. (2015)	0.3	$0.4r_p$	$2.75 \times 10^{-8} (\sim \lambda_g)$
Morris et al. (2016b)	0.3	$0.4r_p$	$2.75 \times 10^{-8} (\sim \lambda_g)$
Lattanzi and Hrenya(2016)	0.2	$0.4r_p$	$2.75 \times 10^{-8} (\sim \lambda_g)$
Lu et al.(2017)	1	$1.08r_p$	1×10^{-6}
Wang et al.(2019)	1	$0.2r_p$	Not given

In static or packed systems, the value of S has a more significant impact on the total amount of heat transfer compared to δ_f , and a large value is not recommended for static or dense particulate systems (Morris et al, 2015).

In dynamic or dilute systems, the results show strong dependence on the selected value of δ_f , but not on S (Lattanzi & Hrenya, 2017).

Although due attention must be given to these parameters, there is no guideline for selecting their values, so different justifications for the choice are found in the literature.

Other Conduction Models

Model by Vargas & McCarthy (2002)

Considers stagnant interstitial fluids (liquid + gas) in packed beds, separating the heat conduction through the liquid and gas phases between contacting particles (i.e. Q_{cpf}).

Applicable for low Reynolds number ($Re \ll 1$), high particle conductivities ($k_{pf} \gg 1$), and identical particles.

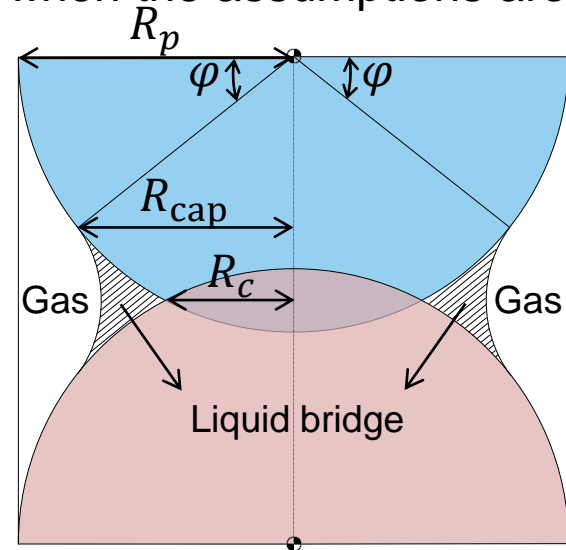
Depends on physical-chemical properties of particles obtained from the literature.

Investigated the dependency of the results with gas pressure, external load and saturation level: good agreement with experiments, when the assumptions are valid.

Assumes unidirectional heat flow and a liquid bridge between contacting particles, with a fixed filling angle φ for all contacts.

$$Q_{pfp} = \left(\frac{k_l A_l}{l_l} + \frac{k_g^* A_g}{l_g} \right) (T_j - T_i)$$

R_c is compute from Hertz theory for static loading



Other Conduction Models

Model by Vargas & McCarthy (2002)

Surface areas exposed to liquid and gas:

$$A_c = \pi R_c^2$$

$$A_l = 4\pi R_p^2 \left(\left(\frac{\pi}{2} - \varphi \right) \tan \varphi - 1 + \cos \varphi \right) \left(\frac{1 - \cos \varphi}{\cos \varphi} \right) - A_c$$

$$A_g = 2\pi R_p^2 - A_l - A_c$$

Characteristic average lengths over which the fluxes apply:

$$l_l = \frac{R_{\text{cap}} R_p - 1/2 \left(\varphi R_p^2 + R_{\text{cap}} \sqrt{R_p^2 - R_{\text{cap}}^2} \right)}{R_{\text{cap}} - R_c}$$

$$l_g = \frac{R_p^2 (1 - \pi/4)}{R_p - R_c} - l_l$$

$$R_{\text{cap}} = \sqrt{R_p^2 (1 - \cos \varphi) (1 + \cos \varphi)}$$

Other Conduction Models

Model by Vargas & McCarthy (2002)

Modified conductivity of gas phase appropriate to use over finite lengths:

$$k_g^* = k_g / (1 + M/l_g)$$

Where:

$$M = \left(\frac{2 - ac_i}{ac_i} + \frac{2 - ac_j}{ac_j} \right) \frac{\zeta}{\zeta + 1} \frac{1}{P_r} \omega$$

$$P_r = \frac{c_g \mu_g}{k_g} \quad (\text{Prandtl number})$$

$$\omega = \frac{k_B T}{\sqrt{2} \pi d_g^2 P_g}$$

$\zeta \rightarrow$ Ratio of specific heats

$ac_i \rightarrow$ Thermal accommodation coefficient at particle surface: empirical parameter obtained from literature data

$P_g \rightarrow$ Gas pressure

$d_g \rightarrow$ Gas molecule diameter

$k_B \rightarrow$ Boltzman constant (1.3806×10^{-23})

$\omega \rightarrow$ Molecular mean free-path of gas

Molecule collision regime: The mean free-path is small w.r.t. mean separation distance ($k_g^* = k_g$).

Free molecule conduction regime: The mean free-path is large w.r.t. mean separation distance ($k_g^* \sim P_g$).

(up to atm pressure, this regime was observed in some gases, e.g. Helium, so the results vary with the interstitial gas pressure)

Other Conduction Models

Model by Vargas & McCarthy (2002)

Interstitial fluid with only gas: $\varphi = A_l = l_l = 0$

$$\left. \begin{aligned} A_g &= 2\pi R_p^2 - \pi R_c^2 \\ l_g &= \frac{R_p^2(1 - \pi/4)}{R_p - R_c} \end{aligned} \right\} Q_{pfp} = k_g^*(T_j - T_i) \frac{2\pi \left(1 - 1/2 (R_c/R_p)^2\right) (R_p - R_c)}{1 - \pi/4}$$

Interstitial fluid with only liquid: $\varphi = \pi/2$ (as a limit)

$$\left. \begin{aligned} A_l &= 4\pi R_p^2 - \pi R_c^2 \\ l_l &= \frac{R_p^2(1 - \pi/4)}{R_p - R_c} \end{aligned} \right\} Q_{pfp} = k_l(T_j - T_i) \frac{4\pi \left(1 - 1/2 (R_c/R_p)^2\right) (R_p - R_c)}{1 - \pi/4}$$

Low Stiffness Correction Models

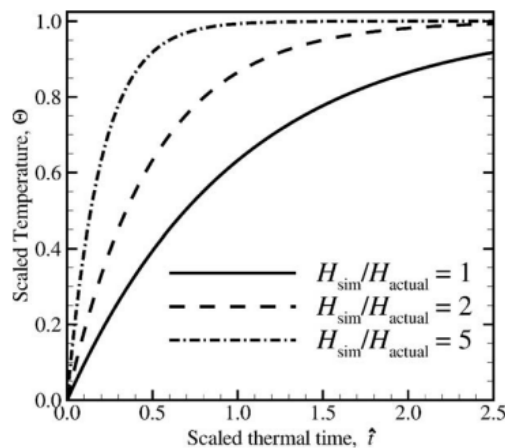
In DEM simulations, it is common to use a low value of Young modulus, compared to the real value, to allow larger time steps and decrease computational time.

It usually does not affect much the kinematics of the particles (Morris et al, 2016a).

However, it leads to a larger contact area and collision time, which increases the contact heat transfer.

Some correction factors have been developed to mitigate this problem and allow the use of low a Young modulus while obtaining realistic heat transfer values.

Nevertheless, other problems can arrive from low stiffness of particles, such as the change in porosity distribution.



Morris et al (2016a)

Analytic scaled temperature rise (Eq. 7) vs. a dimensionless thermal relaxation time for a particle resting on a heated surface.

The level of softening is indicated by value H_{sim}/H_{actual} ; $H_{sim}/H_{actual} = 1$ refers to non-softened case.

Low Stiffness Correction Models

Model by Zhou et al (2010)

Proposed a correction coefficient of the maximum contact radius based on the real and adopted values of the Young modulus.

The coefficient is based on the maximum contact area of Hertz theory for an elastic collision between two spheres.

The reduced contact radius is expressed as:

$$R_c^{\text{cor}} = \left(\frac{\bar{E}}{\bar{E}_{\text{real}}} \right)^{1/5} R_c^{\text{max}}$$

Where \bar{E}_{real} is calculated as \bar{E} but with real value of Young modulus.

It has been reported to work for both packed and fluidized beds.

The reduced radius is then used in the formulas of contact particle-particle conduction, in place of the overestimated contact radius.

Low Stiffness Correction Models

Model by Lu et al (2017)

The correction coefficient of Zhou et al (2010), based on Hertz theory, has been extended to the linear spring-dashpot model.

The reduced contact radius is expressed as:

$$R_c^{\text{cor}} = \left(\frac{K_n R_c}{K_{HZ, \text{real}}} \right)^{2/3}$$

Where k_n and $k_{HZ, \text{real}}$ are, respectively, the normal spring constant used in the simulation and the spring constant derived from the real value of the Young modulus (see [appendix A](#), for the expression of K_{HZ}).

The reduced radius is then used in the formulas of contact particle-particle conduction, in place of the overestimated contact radius.

Low Stiffness Correction Models

Model by Morris et al (2016a)

Two correction factors to adjust both the overestimated contact area and contact time.

Based on the Batchelor & O'Brien (1977) model ($Q_{pp} = 2k_p R_c^{\text{htz}} \Delta T$), by applying both correction coefficients:

$$Q_{cpp} = 2k_p \underbrace{\left(\frac{F_n \bar{R}}{\bar{E}_{\text{real}}} \right)^{1/3}}_{\substack{\text{area} \\ \text{correction}}} \underbrace{\left(\frac{t_{c,\text{real}}}{t_c} \right)^{2/3}}_{\substack{\text{time} \\ \text{correction}}} (T_j - T_i)$$

Where F_n and t_c are computed according to the contact law, and \bar{E}_{real} and $t_{c,\text{real}}$ are computed with the real values of the material properties.

In static systems, the time correction term (ratio of collision times) is equal to unity, and only the area correction term is applied.

This correction performs well for moderately dense flows, but for dense flows it is not recommended as the time correction was derived for a binary collision.

3 – Convective Heat Transfer

Heat Convection Mechanisms

Thermal convection

Related to fluid motion: heat is carried along with the flow.

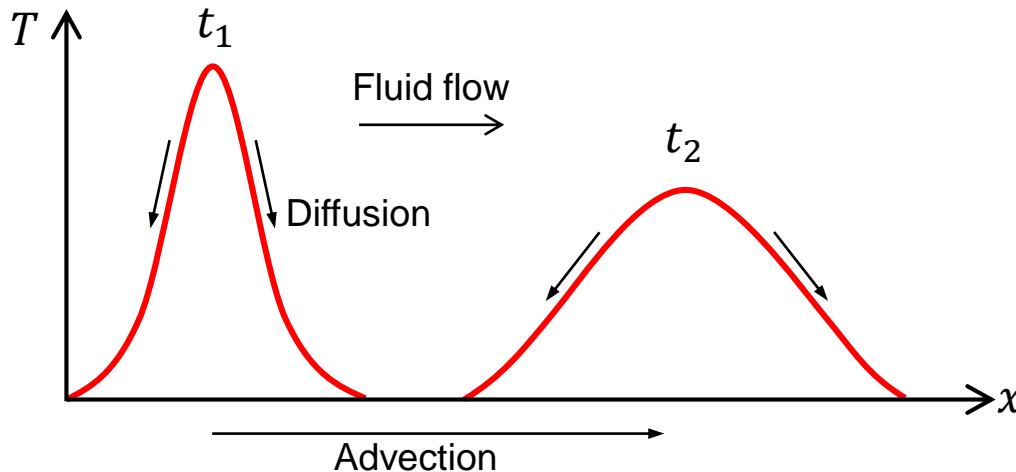
→ **Natural convection:** Fluid motion caused by density change.

→ **Forced convection:** Fluid motion forced by external agents.

The fluid motion induces heat transfer by:

→ **Advection:** Heat transfer by the bulk motion of the fluid.

→ **Diffusion:** Heat transfer by the collision of molecules due to temperature gradient.



$$\text{Total convective heat transfer} \\ = \text{Advection} + \text{Diffusion}$$

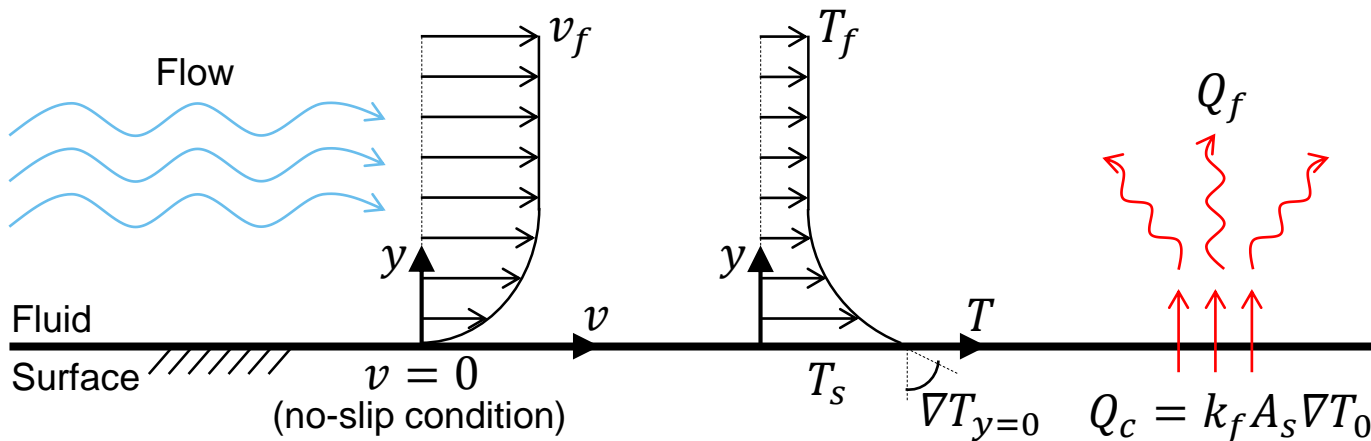
Heat Convection Mechanisms

Fluid-solid convection

The total convective heat transfer is expressed by Newton's law of cooling, in which a convective coefficient relates the rate of heat transfer with the solid's surface area and the temperature difference between the surface and the fluid (away from the surface):

$$Q_f = hA_s(T_s - T_f)$$

The convective heat transfer coefficient is application-dependent: it is influenced by flow conditions (velocity, direction, type), problem geometry (system shape / size), etc.



In the interface, heat is transferred by conduction. Then, it is propagated through the fluid by diffusion and advection.

$$hA_s \Delta T = k_f A_s \nabla T_0$$

$$h = \frac{k_f \nabla T_0}{\Delta T}$$

The *Nusselt* number (Nu) is then used to allow a general description of convection.

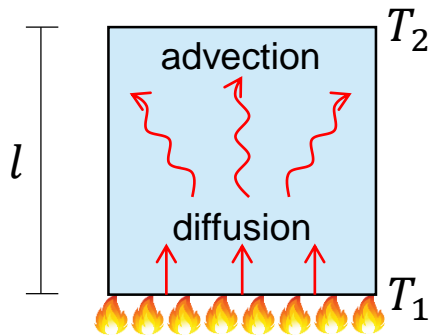
Dimensionless Numbers

Nusselt number

Dimensionless number of the ratio between the total convective heat transfer and a fictitious pure conduction situation (as if the fluid was completely still).

$$N_u = \frac{Q_f}{Q_c} = \frac{hA_s\Delta T}{k_f A_s \Delta T / l} = \frac{hl}{k_f} \left\{ \begin{array}{l} \text{Stagnant fluid} \rightarrow N_u = 1 \quad (\text{heat diffusion only}) \\ \text{Laminar flow} \rightarrow N_u = 1 \sim 10 \\ \text{Turbulent flow} \rightarrow N_u = 10^2 \sim 10^3 \quad (\text{heat advection dominates}) \end{array} \right.$$

Analogous to the [Biot number](#), but employing the thermal conductivity of the fluid, instead of the solid, thus being a comparative measure of the advection and diffusion contributions to the total convective heat transfer within the fluid.



$$\left. \begin{array}{l} \text{Total convection: } Q_f = hA_s\Delta T \\ \text{Pure conduction: } Q_c = \frac{k_f}{l} A_s\Delta T \end{array} \right\} N_u = \frac{hl}{k_f} = \frac{\nabla T_0}{\Delta T / l}$$

The temperature profile, thus the gradient, is not known in most of the situations.

There are many correlations to relate N_u with flow conditions, problem geometry, etc. Most of them involve the *Reynolds* and *Prandtl* numbers, and the average porosity.

Dimensionless Numbers

Reynolds number

Dimensionless number of the ratio between inertial and viscous forces in a fluid flow.

Helps to predict the flow characteristics in different scenarios.

Depends on specific application properties: flow velocity and characteristic length.

$$R_e = \frac{\rho_f v_f l}{\mu_f} \left\{ \begin{array}{l} \text{Low } R_e \rightarrow \text{Viscous forces dominate} \\ \text{(laminar flows)} \\ \text{High } R_e \rightarrow \text{Inertial forces dominate} \\ \text{(turbulent flows)} \end{array} \right.$$

Prandtl number

Dimensionless number of the ratio between momentum and thermal diffusivities.

Depends only on fluid properties: heat capacity, viscosity and conductivity.

$$P_r = \frac{c_f \mu_f}{k_f} \left\{ \begin{array}{l} P_r \ll 1 \rightarrow \text{Thermal diffusivity dominates} \\ \text{(heat diffuses quicker)} \\ P_r \gg 1 \rightarrow \text{Momentum diffusivity dominates} \\ \text{(velocity diffuses quicker)} \end{array} \right.$$

Convection Correlations

Predominant correlations for particle-fluid convection in DEM simulations (Peng, 2020):

Authors	Correlation	Conditions
Ranz & Marshall (1952)	$N_u = 2 + 0.6R_e^{1/2}P_r^{1/3}$	$R_e = 1.0 \sim 10^4$ $P_r = 0.6 \sim 380$
Whitaker (1972)	$N_u = 2 + \left(0.4R_e^{1/2} + 0.06R_e^{2/3}\right)P_r^{2/5} \left(\frac{\mu_f}{\mu_{fs}}\right)^{1/4}$	$R_e = 3.5 \sim 7.6 \times 10^4$ $P_r = 0.71 \sim 380$ $\mu_f/\mu_{fs} = 1.0 \sim 3.2$
Gunn (1978)	$N_u = (7 - 10\varepsilon + 5\varepsilon^2) \left(1 + 0.7R_e^{1/5}P_r^{1/3}\right) + (1.33 - 2.4\varepsilon + 1.2\varepsilon^2)R_e^{7/10}P_r^{1/3}$	$R_e < 10^5$ $R_a < 10^9$ All P_r
Li & Mason (2000)	$N_u = \begin{cases} 2 + 0.6\varepsilon^m R_e^{1/2} P_r^{1/3} & R_e < 200 \\ 2 + \varepsilon^m \left(0.5R_e^{1/2} + 0.02R_e^{4/5}\right) P_r^{1/3} & R_e < 1500 \\ 2 + 0.000045\varepsilon^m R_e^{9/5} & R_e > 1500 \end{cases}$	$m = 3.50 \rightarrow$ dilute $m = 4.75 \rightarrow$ dense $P_r = 0.7 \sim 1.0$ $\varepsilon = 0.35 \sim 1.0$

μ_{fs} : Fluid's dynamic viscosity at surface's temperature (may be assumed as $\mu_{fs} = \mu_f$)

Convection Correlations

- Most of the correlations are empirical or semi-empirical.
- In DEM simulations, most of them are for flows past a single sphere.
- A given correlation is not generally applicable to different problems and / or conditions, so it must be selected with due care.
- The correlations can be grouped based on their application to systems with different solid concentration: dense systems, dilute systems, pneumatic systems.
- The correlation by Ranz & Marshall has become the foundation for many succeeding models. It is the most common for smooth spheres and has been employed in both dilute and dense DEM systems.
- The correlation by Gunn is mainly for relatively dilute systems.
- The correlation by Li & Mason was developed for pneumatic transport.
- Many other correlations are available in the literature, although not widely used as the ones listed above.

Calculation Procedure

Flowing fluid through DEM particles

To account for the convective heat transfer between particles and the surrounding fluid, a suited correlation is employed to determine N_u for the specific problem conditions.

The value of N_u is then used to estimate the convection coefficient and the rate of heat transfer (for spheres, the characteristic length is taken as the diameter: $l_i = 2R_i$):

$$N_u(R_e, P_r, \varepsilon) \rightarrow h_i = \frac{N_u k_f}{2R_i} \rightarrow Q_{f,i} = h_i A_{s,i} (T_f - T_p) = \frac{N_u k_f}{2R_i} A_{s,i} \Delta T = 2\pi R_i k_f N_u \Delta T$$

The basic properties needed for the fluid and for characterizing the flow are:

- Fluid properties: k_f, ρ_f, c_f, μ_f
- Flow properties: v_f, l_i (for R_e)

These properties should be known locally, around each particle. For simplicity, in most DEM simulations, their given values are assumed to hold for all particles.

Calculation Procedure

Stagnant fluid around DEM particles

For nearly stationary particles within a stagnant interstitial fluid, R_e vanishes.

This leads to a constant value of N_u ($N_u = 2$, in most correlations).

The fact that $N_u \neq 1$ in this case indicates that advection still plays a role even though the fluid is considered still around the particle. The advection effect is due to the natural convection that occurs near the surface and is considered by the correlation formulas.

$$N_u = 2 \quad \rightarrow \quad h_i = \frac{k_f}{R_i} \quad \rightarrow \quad Q_{f,i} = \frac{k_f}{R_i} A_{s,i} (T_f - T_p) = 4\pi R_i k_f \Delta T$$

In both cases of flowing and stagnant fluid, an assumption is that the effect of particle rotation is neglected for computing N_u , and thus h_i and $Q_{f,i}$.

Furthermore, a 1-way thermal coupling between the interstitial fluid and the particles is normally assumed: the fluid temperature affects the particles temperature, by means of convective heat transfer, but not the opposite way.

4 – Radiative Heat Transfer

Heat Radiation Mechanisms

Thermal radiation

Heat transfer by emission of electromagnetic waves, as a consequence of thermal agitation of molecules, without the need for a transmitting medium.

All heated bodies (above 0K) emit thermal radiation.

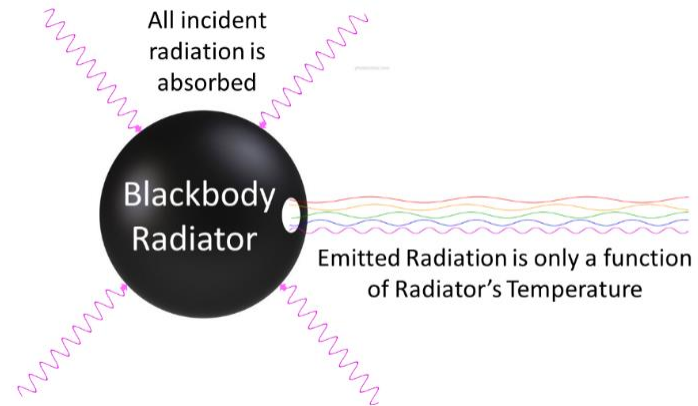
Heat transfer occurs among the surface of the bodies.

For a black body*, the radiation power can be expressed by Stefan-Boltzmann law:

$$\sigma = 5.6703 \cdot 10^{-8} [W/m^2K^4]$$

$$I = \sigma T_s^4$$

$$Q_{rbb} = A_s I$$



* Hypothetical body that absorbs all incident thermal radiation that falls on its surface, and emits radiation on the same rate (perfect absorber and emitter).

Heat Radiation Mechanisms

Net radiation with surrounding environment

The radiation emitted by real surfaces is calculated as a fraction of the black body radiation, given by an emissivity coefficient ($\epsilon = 0 \sim 1$), which is a surface property:

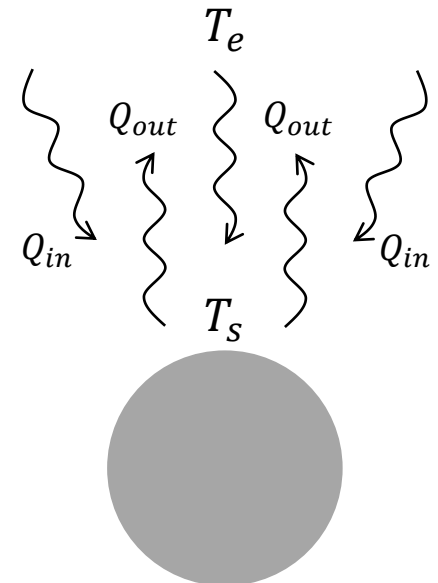
$$Q_{out} = \epsilon Q_{rbb} = \epsilon A_s \sigma T_s^4$$

The incident radiation (irradiation) from the surroundings (whose average temperature is T_e) is partially reflected, absorbed and transmitted. The absorbed fraction is given by an absorptivity coefficient which, under the “grey body” assumption, is equal to the emissivity coefficient:

$$Q_{in} = \epsilon A_s \sigma T_e^4$$

The net rate of radiative heat transfer to a body is then:

$$Q_r = \epsilon A_s \sigma (T_e^4 - T_s^4)$$

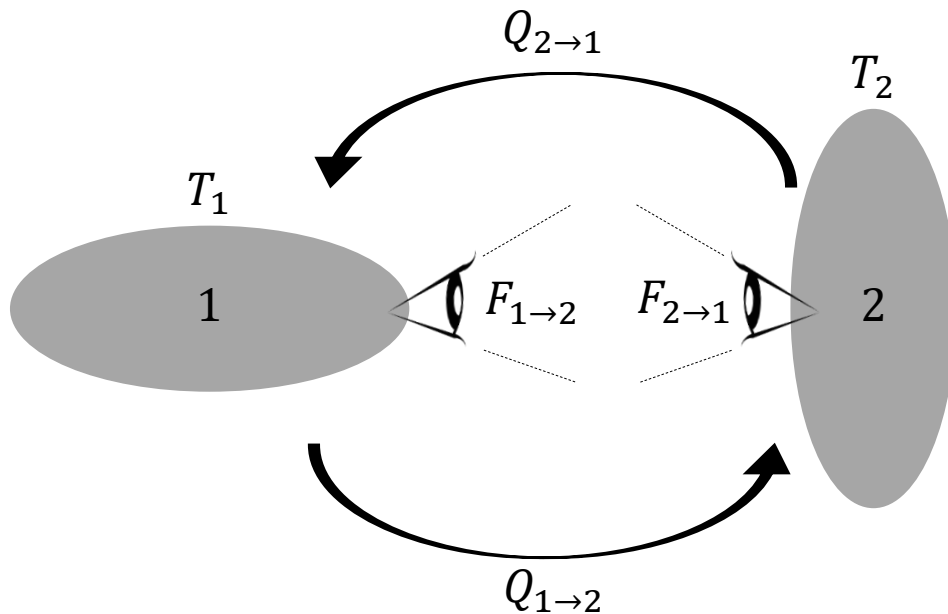


Heat Radiation Mechanisms

Net radiation with other surfaces

The irradiation that falls on an object's surface may come from any other surface to which the analyzed object is exposed to.

The net radiative heat transfer from one surface to another depends on their shapes and relative position, which is accounted by view factors $F_{i \rightarrow j}$.



$$Q_1 = Q_{2 \rightarrow 1} - Q_{1 \rightarrow 2}$$

$$Q_1 = \epsilon F_{2 \rightarrow 1} A_{s,2} \sigma T_2^4 - \epsilon F_{1 \rightarrow 2} A_{s,1} \sigma T_1^4$$

By reciprocity: $F_{1 \rightarrow 2} A_{s,1} = F_{2 \rightarrow 1} A_{s,2}$

$$Q_1 = \epsilon F_{1 \rightarrow 2} A_{s,1} \sigma (T_2^4 - T_1^4)$$

DEM Radiation Models

Because of the 4th-order dependency on the temperature, the amount of heat transfer increases significantly as temperature increases, but becomes relevant only at high temperatures (typically > 700K – Zabrodsky, 1966).

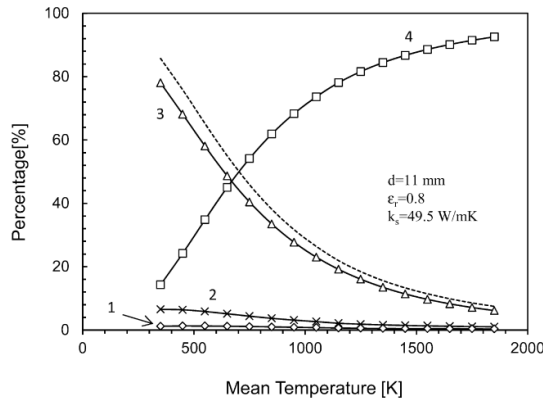


Figure 13. Effect of mean bed temperature on the relative contributions of the heat transfer mechanisms to the overall heat transfer: line 1, heat conduction Q_{nsf} ; line 2, heat conduction Q_{csf} ; line 3, heat conduction Q_{css} ; line 4, the solid–solid radiation between particle surfaces; dashed-line, the percentage of total conduction.

Cheng et al (2013)

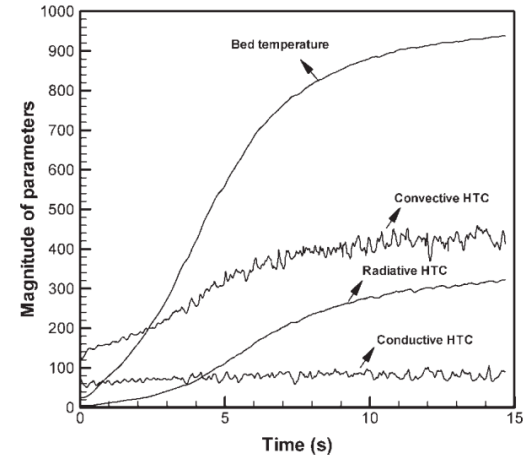


Figure 16. Thermal behavior of bed particles under the condition of gas inlet temperature 1,000°C, and superficial velocity 3.2 m/s.

Zhou et al (2009)

Radiation is more challenging and computationally expensive to be considered than other heat transfer mechanisms, thus it is generally neglected at lower temperatures.

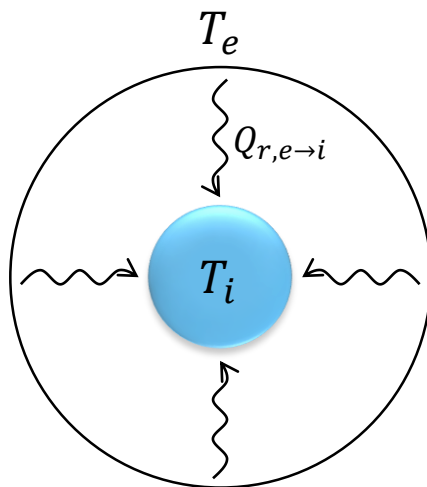
In solid-liquid systems, it disappears, so it is only considered in solid-gas systems (Kunii & Smith, 1960).

DEM Radiation Models

Modeling approaches

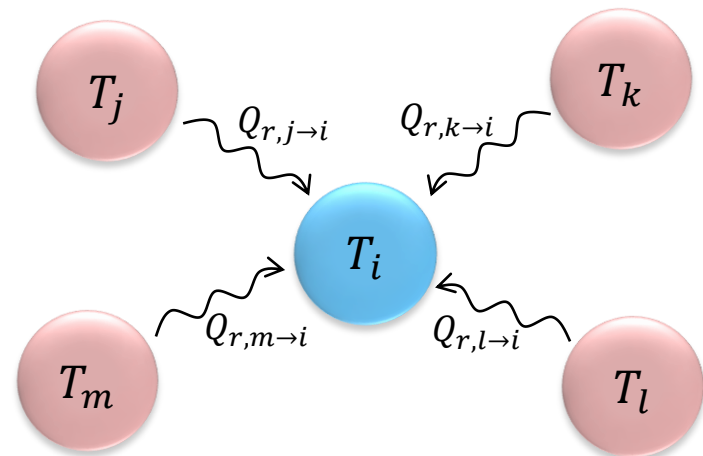
Continuum

Simplified approach based on average local properties of the model. It assumes a representative environment temperature around each particle to which the particle is exposed. There is no need to compute view factors (computationally cheaper).



Discrete

Computes the heat transfer between the surfaces of individual particles based on the solution of view factors. It provides more accurate results but it is more computationally expensive. (currently not covered in this presentation)



DEM Radiation Models

Continuum model

A spherical volume of radiative influence is defined around each particle (the radius of the spherical domain is normally set as $3R_i$).

An environment temperature is assumed for the enclosing surface, taken as the volume averaged temperature of the n_p surrounding particles and the fluid as:

- Zhou et al (2009):
$$T_e = \varepsilon T_f + (1 - \varepsilon) \frac{1}{n_p} \sum_{j=1}^{n_p} T_j$$

- Krause et al (2017):
$$T_e = \left(\frac{\sum_j \varepsilon_j A_j \sigma T_j^4 / 2}{\sum_j \varepsilon_j A_j \sigma / 2} \right)^{1/4}$$
 It assumes that if the centroid of another particle lies within the spherical domain, the half surface of this particle is considered.

The radiative heat transfer between each particle and the surrounding environment is:

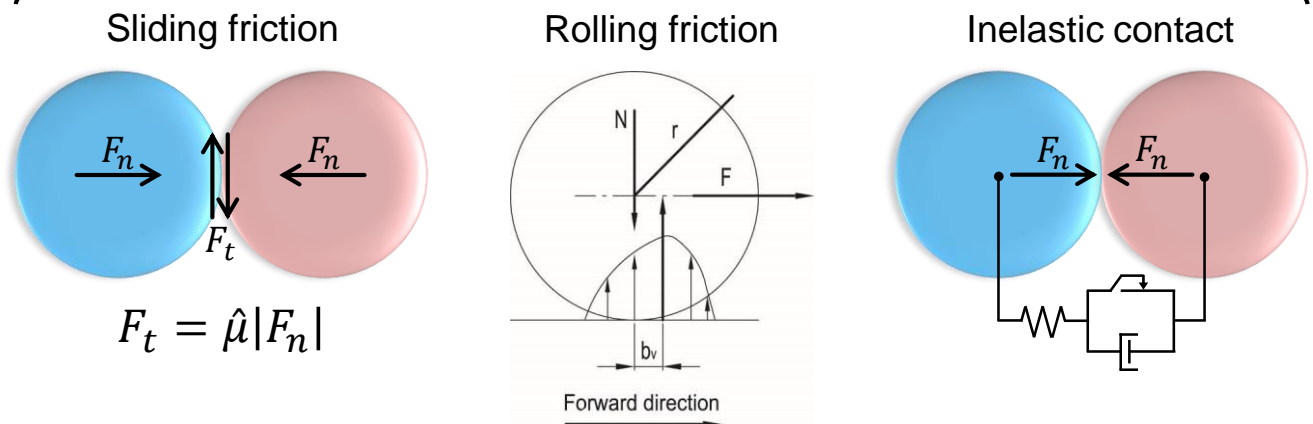
$$Q_{r,i} = \varepsilon_i A_{s,i} \sigma (T_e^4 - T_i^4)$$

5 – Heat Generation

Heat Generation

Besides heat flow by conduction, convection and radiation due to temperature gradient, heat might also be generated by several mechanisms:

- Mechanical energy dissipation:
 - Friction (sliding & rolling)
 - Inelastic contact (viscosity & plasticity)
- Phase change
- Chemical reactions
- Biological activity



Heat Generation

Mechanical energy dissipation

The mechanical energy of particles is partially dissipated during interactions.

Each energy dissipation mechanism is related to a dissipative force or torque.

The calculation of dissipative forces/torques depends on the contact model adopted.

$$\text{Dissipation Energy} = \text{Dissipative Force} \times \text{Distance}$$

$$\text{Dissipation Power } (P) = \frac{\text{Dissipation Energy}}{\text{Time}} = \text{Dissipative Force} \times \text{Velocity}$$

A fraction of the dissipation power is converted into heat: $Q_g = \chi P$

The heat conversion coefficient is an adjustable parameter ($0 \leq \chi \leq 1$).

Most of the time, it is assumed that all dissipation power is converted into heat ($\chi = 1$).

Archard (1958): “Nearly all the energy dissipated by friction appears as heat”.

Heat Generation

Sliding friction dissipation

Energy is dissipated by the relative sliding between particles.

Frictional power from Coulomb's friction is converted into heat:

$$Q_g = \chi |\hat{\mu} F_n \dot{\delta}_t| \quad \left\{ \begin{array}{l} \hat{\mu} \rightarrow \text{Dynamic friction coefficient} \\ F_n \rightarrow \text{Normal contact force} \\ F_t \rightarrow \text{Tangential contact force} \\ \dot{\delta}_t \rightarrow \text{Tangential (sliding) relative velocity between particles} \end{array} \right.$$

or

$$Q_g = \chi |F_t \dot{\delta}_t|$$

Rolling friction dissipation

Energy dissipation from asymmetrical normal traction distribution on the contact area.

$$Q_g = \chi |\tau \omega_r| \quad \left\{ \begin{array}{l} \tau \rightarrow \text{Rolling friction torque} \\ \omega_r \rightarrow \text{Relative rotational velocity} \end{array} \right.$$

Heat Generation

Inelastic dissipation

Energy dissipated by the viscous (damping) and / or plastic components of the contact force between particles in the normal and tangential relative directions:

$$\begin{array}{l} \text{Heat generated from damping:} \\ Q_g = \chi(F_n^{vis} \dot{\delta}_n + F_t^{vis} \dot{\delta}_t) \\ \\ \text{Heat generated from plasticity:} \\ Q_g = \chi(F_n^{pl} \dot{\delta}_n + F_t^{pl} \dot{\delta}_t) \end{array} \left\{ \begin{array}{l} F_n^{vis} \rightarrow \text{Viscous component of normal contact force} \\ F_t^{vis} \rightarrow \text{Viscous component of tangential contact force} \\ F_n^{pl} \rightarrow \text{Plastic component of normal contact force} \\ F_t^{pl} \rightarrow \text{Plastic component of tangential contact force} \\ \dot{\delta}_n \rightarrow \text{Normal relative velocity between particles} \\ \dot{\delta}_t \rightarrow \text{Tangential relative velocity between particles} \end{array} \right.$$

Heat Generation

Partition coefficient

The heat generated at the contact interface is absorbed by both particles.

The fraction of heat absorbed by each particle is given by a partition coefficient ψ :

$$Q_g = Q_{g,i} + Q_{g,j} \begin{cases} Q_{g,i} = \psi_i Q_g \\ Q_{g,j} = (1 - \psi_i) Q_g \end{cases}$$

Several formulas are proposed for the partition coefficient:

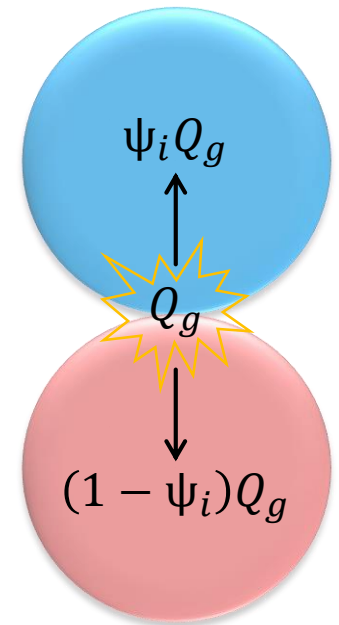
Váradi et al (1996):
$$\psi_i = \frac{k_i}{k_i + k_j}$$

Vernotte (1956), Rojek (2014):
$$\psi_i = \frac{e_i}{e_i + e_j}$$

Mokrani & Bourouga (2005):
$$\psi_i = \frac{1}{2} \left(\frac{k_i}{k_i + k_j} + \frac{\hat{\rho}_i}{\hat{\rho}_i + \hat{\rho}_j} \right)$$

e = thermal effusivity ($\sqrt{\rho c k}$)

$\hat{\rho}$ = electrical resistivity



If both particles have the same material:

$$\psi_i = 0.5$$

Heat Generation

Sun et al (2022):

Numerical simulation of a drop-weight over a layer of particles.

The sources of heat generation are:

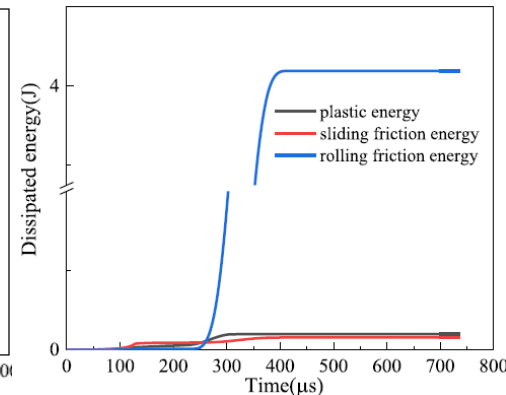
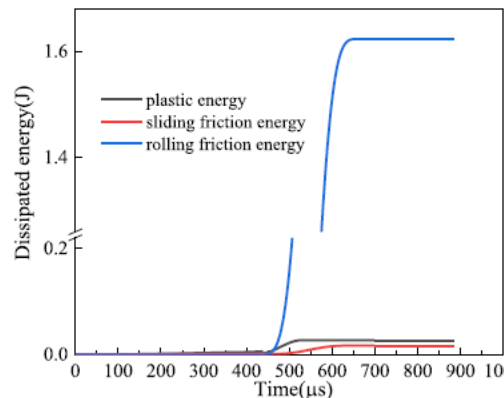
- Sliding friction
- Rolling friction
- Plastic deformation (from an elasto-plastic model for normal contact force)

Conversion coefficient from the total energy dissipation to heat: $\chi = 0.9$.

(value established for plastic deformation of metals according to Hodowany et al, 2000)

Sliding friction and plastic deformation are relevant in early stages.

Then, the main contribution of energy dissipation is largely from rolling friction.



Heat Generation

Hu et al (2021):

Numerical simulation (pure DEM) of heat generation on a rotating drum with blades.

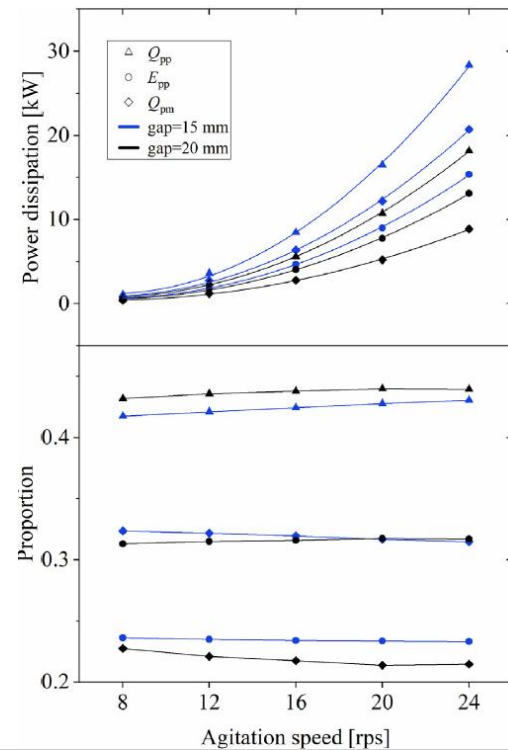
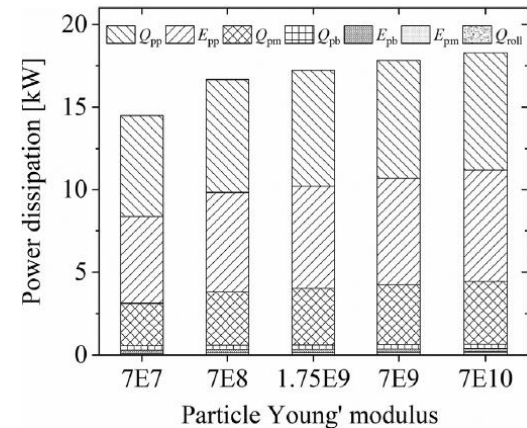
The sources of heat generation are:

- Sliding friction
- Rolling friction
- Inelastic contact (damping in normal & tangential directions)

The partition coefficient applies only to friction heat generation.

Studied the effect of a reduced stiffness on energy dissipation: The energy loss varies little in the range $7e8$ – $7e10$ Pa. However, it decreases significantly for $7e7$ Pa.

The 3 dominant energy dissipation mechanisms are the friction between particles and particles-walls, and the damping between particles (in the graphs: Q_{pp} , Q_{pm} , E_{pp} , respectively).



Heat Generation

Sun et al (2018):

Numerical (DEM+CFD) and experimental analysis of heat generation on a rotating drum with blades.

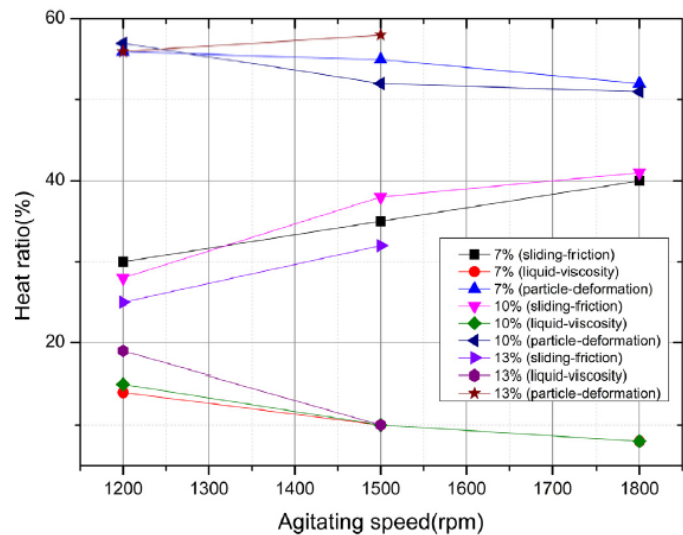
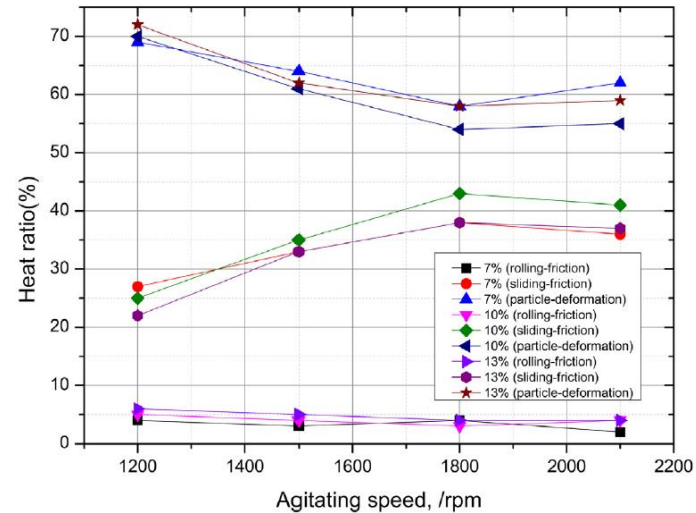
The sources of heat generation are:

- Sliding friction
- Rolling friction
- Viscous force from inter-particle damping (named as “particle deformation”)
- Viscous force from fluid damping by liquid bridges in wet particles.

The partition coefficient applies to friction only.

Studied the influence of each heat generation mechanism in dry and wet (by oil) systems.

Inter-particle damping presents a greater contribution.



Heat Generation

Al-Arkawazi (2017):

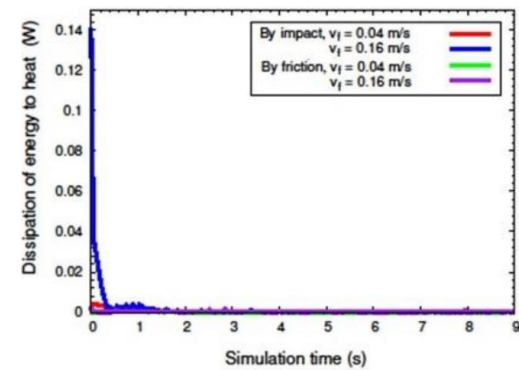
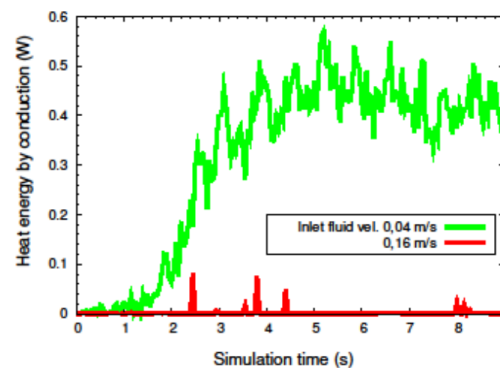
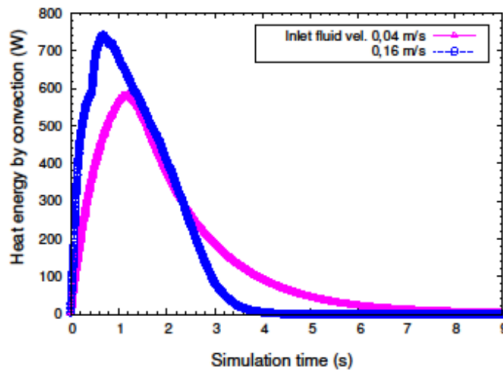
Thermomechanical simulation (DEM+CFD) of fluidized beds.

Heat generation by **friction** and **kinetic energy dissipation** during collisions.

Kinetic energy dissipation results from velocities difference before and after collision:

$$\Delta U = \Delta U_i + \Delta U_j = \left\{ \begin{array}{l} \Delta U_i = \frac{1}{2} \left(m_i \left((v_i^{t+t_c})^2 - (v_i^t)^2 \right) + I_i \left((\omega_i^{t+t_c})^2 - (\omega_i^t)^2 \right) \right) \\ \Delta U_j = \frac{1}{2} \left(m_j \left((v_j^{t+t_c})^2 - (v_j^t)^2 \right) + I_j \left((\omega_j^{t+t_c})^2 - (\omega_j^t)^2 \right) \right) \end{array} \right\} \text{Heat generation due to collision: } Q_g = \frac{\Delta U}{t_c}$$

The contribution of heat generation mechanisms (friction and collision) is very small compared to the heat transfer mechanisms (conduction and convection):



Heat Generation

Rojek (2014):

Simulation of rock cutting with DEM as a discretization tool to model a continuous rock.

Heat is generated only by **sliding friction**, with a conversion coefficient of $\chi = 0.85$.

Richard et al (2008), Terreros et al (2009):

DEM used to model a “third body” at the contact interface of sliding surfaces and Friction Steel Welding.

Instead of estimating a friction coefficient, consider the **dissipation due to damping** as the main source of heat generation.

All dissipated energy is converted into heat, and it is equally divided between elements.

The heat generated from the viscous component of the normal force is given by:

$$Q_g = F_n^{vis} \dot{\delta}_n = 2\mu\sqrt{K_n\bar{m}}\dot{\delta}_n^2$$

$$Q_{g,i} = Q_{g,j} = 0.5Q_g$$

Heat Generation

Nguyen et al (2009a, 2009b, 2020):

Thermomechanical simulations of the shearing of granular materials confined between parallel plates and the discharge of silos.

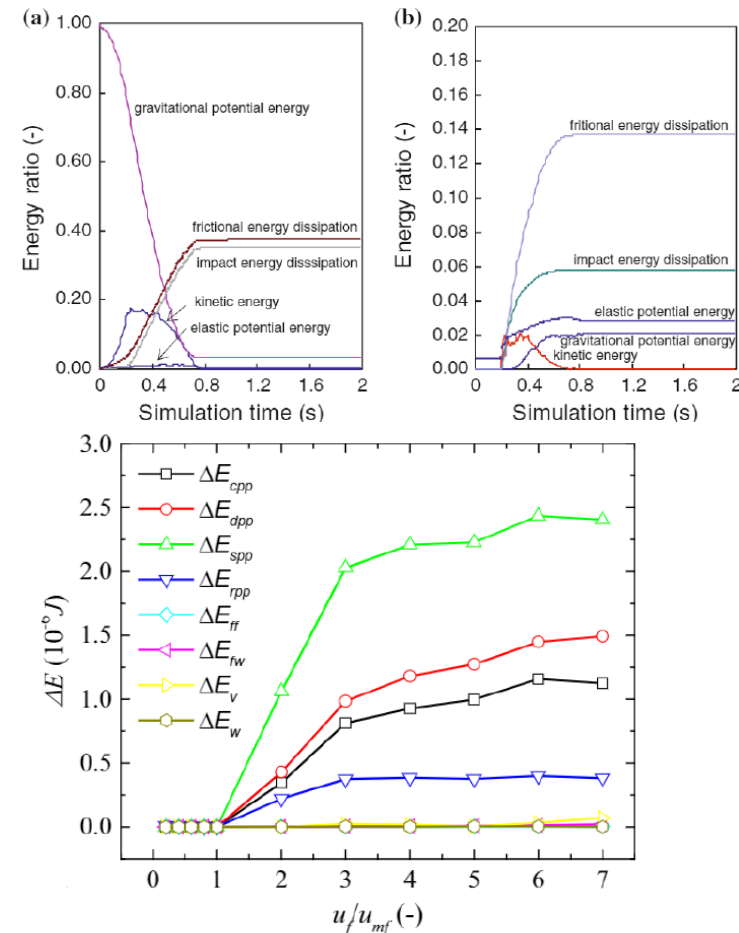
Heat is generated only by **sliding friction**.

Wu et al (2007), Hou et al (2017):

Other numerical studies focus only on the variation and dissipation of energy in granular systems, but with no heat involved.

In the impact of a particle stream onto a particle bed, the sliding friction and damping force led to most of the energy dissipation.

In fluidized beds, the energy dissipation due to viscous drag force is dominant.



Appendix A – Contact Mechanics

Contact Mechanics

Effective parameters used for the contact between 2 spheres

$$\bar{R} = \left(\frac{1}{R_i} + \frac{1}{R_j} \right)^{-1} = \frac{R_i \cdot R_j}{(R_i + R_j)}$$

$$\bar{m} = \left(\frac{1}{m_i} + \frac{1}{m_j} \right)^{-1} = \frac{m_i \cdot m_j}{(m_i + m_j)}$$

$$\bar{k} = \left(\frac{1}{k_i} + \frac{1}{k_j} \right)^{-1} = \frac{k_i \cdot k_j}{(k_i + k_j)}$$

$$\bar{E} = \left(\frac{1 - (\nu_i)^2}{E_i} + \frac{1 - (\nu_j)^2}{E_j} \right)^{-1}$$

A wall can be treated as a particle with $R_{\text{wall}} = m_{\text{wall}} = \infty$

Contact Mechanics

Hertz theory

Accurately describes the elastic behavior of spheres in contact or colliding, therefore it is normally used for the heat transfer models by contact conduction.

Models the contact of elastic and smooth solids based on the linear theory of elasticity (Hertz, 1882; Timoshenko & Goodier, 1951; Johnson, 1985).

Assumptions:

- Perfectly elastic bodies (strains are sufficiently small to consider linear elasticity).
- Perfectly smooth surfaces (i.e. frictionless – only normal pressure).
- Parabolic profile of stresses over the contact area, which is assumed as circular.
- The contact area must be small compared to the dimensions of each body and to the relative radii of curvature of each surface.

Contact Mechanics

Contact parameters – static loading by Hertz

The case of 2 spheres brought and kept into contact by a normal force F_n .

Contact radius:
$$R_c^{\text{htz}} = \left(\frac{3 F_n \bar{R}}{4 \bar{E}} \right)^{1/3} = \sqrt{\bar{R} \delta_n}$$

Particle displacement:
(DEM overlap)
$$\delta_n = \frac{(R_c^{\text{htz}})^2}{\bar{R}} = \left(\frac{9 F_n^2}{16 \bar{R} \bar{E}^2} \right)^{1/3}$$

P.S. The relationship between normal force and overlap is:

$$F_n = K_{HZ} \delta_n^{3/2} \quad K_{HZ} = \frac{4}{3} \bar{E} \sqrt{\bar{R}}$$

Contact Mechanics

Contact parameters – quasi-static loading by Hertz

The collinear impact between elastic frictionless bodies follows the static Hertz theory.

Hertz theory was developed for static contact, but it is valid for collisions as long as the impact velocity is small compared to the speed of bulk elastic waves.

It is quasi-static in the sense that the deformation is assumed to be restricted to the vicinity of the contact area and to be given by the static theory.

Gives the solution of the dynamic system for normal collision: $\bar{m}\ddot{\delta}_n + K_{HZ}\delta_n^{3/2} = 0$

Maximum contact radius and overlap: $R_c^{\max} = \left(\frac{15 \bar{m} \bar{R}^2}{16 \bar{E}} \dot{\delta}_n^{0^2} \right)^{1/5}$ $\delta_n^{\max} = \frac{(R_c^{\max})^2}{\bar{R}} = \left(\frac{15 \bar{m}}{16 \sqrt{\bar{R} \bar{E}}} \dot{\delta}_n^{0^2} \right)^{2/5}$

Total collision time: $t_c = 2.87 \left(\frac{\bar{m}^2}{\bar{R} \bar{E}^2 \dot{\delta}_n^0} \right)^{1/5}$ where $t_c^{\max} = \frac{t_c}{2}$

Contact Mechanics

Contact parameters – geometry based

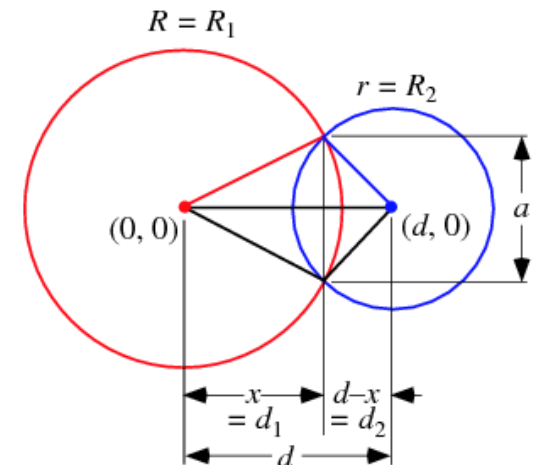
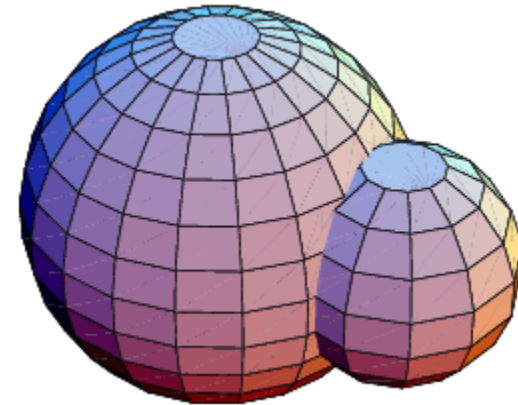
Independent of the contact model and overlap magnitude, computed based on the overlap geometry, which is assumed in DEM.

The contact radius for overlapping circles / spheres is:
(Musser 2011; Zohdi 2013; Weisstein)

$$R_c^{\text{geo}} = \sqrt{R_i^2 - \left(\frac{R_i^2 - R_j^2 + d_{ij}^2}{2d_{ij}} \right)^2}$$

or

$$R_c^{\text{geo}} = \frac{1}{2d_{ij}} \sqrt{4d_{ij}^2 R_i^2 - (d_{ij}^2 - R_j^2 + R_i^2)^2}$$



Nomenclature

Nomenclature

Symbols

a, b, c	Auxiliary parameters for indirect conduction [K/W]	d_{pw}	Distance between centroid of particle i and wall [m]
ac	Thermal accommodation coefficient [-]	dQ	Elementary rate of heat transfer [W]
A	Auxiliary parameters for indirect conduction [-]	d_s	Distance between surfaces of particles [m]
A_c	Contact area [m ²]	D	Distance from particle centroid to separation plane [m]
A_g	Surface area exposed to gas [m ²]	E	Young modulus [Pa]
A_l	Surface area exposed to liquid [m ²]	\bar{E}	Effective Young modulus [Pa]
A_n	Face area of Voronoi polyhedron [m ²]	$F_{i \rightarrow j}$	View factor from i to j [-]
A_p	Cross-section area of thermal pipe [m ²]	F_n	Normal contact force [N]
A_s	Surface area [m ²]	F_t	Tangential contact force [N]
B	Auxiliary parameter for indirect conduction [-]	F_o	Fourier number [-]
B_i	<i>Biot</i> number [-]	G	Shear modulus [Pa]
c	Specific heat capacity [J/(kg.K)]	h	Convective heat transfer coefficient [W/(m ² .K)]
c_f	Specific heat capacity of fluid [J/(kg.K)]	H	Thermal conductance [W/K]
c_g	Specific heat capacity of gas [J/(kg.K)]	\tilde{H}_c	Dimensionless heat flow across contact circle [-]
C	Correction coefficient [-]	\tilde{H}_f	Dimensionless relative heat flow via interstitial fluid [-]
$C_1 - C_4$	Correlation parameters [-]	I	Radiation emissivity power [W/m ²]
$d_f(r)$	Distance for conduction through fluid [m]	k	Thermal conductivity [W/(m.K)]
d_g	Molecule diameter of gas [m]	\bar{k}	Effective thermal conductivity [W/(m.K)]
d_{ij}	Distance between centroids of particles i and j [m]	\tilde{k}	Average thermal conductivity [W/(m.K)]
$d_p(r)$	Distance for conduction within particle [m]	k_B	Boltzmann constant [m ² kg/(s ² K)]
		k_f	Thermal conductivity of fluid [W/(m.K)]

Nomenclature

γ	Dimensionless radius of particle [-]	Q_{cpp}	Rate of heat transfer by conduction due to particle-particle contact [W]
k_g^*	Modified thermal conductivity of gas [W/(m.K)]	Q_{npfp}	Rate of heat transfer by conduction due to non-contact particle-fluid-particle [W]
k_l	Thermal conductivity of liquid [W/(m.K)]	Q_{pfp}	Rate of heat transfer by conduction through the fluid between particles [W]
k_p	Thermal conductivity of particle [W/(m.K)]	Q_{pfw}	Rate of heat transfer by conduction through the fluid between particle and wall [W]
k_{pf}	Ratio of thermal conductivities of particle and fluid [-]	Q_e	Rate of heat transfer by external source [W]
K_n	Normal spring stiffness coefficient [N/m]	Q_f	Rate of heat transfer by fluid convection [W]
K_{hz}	Hertzian spring stiffness coefficient [N/m]	Q_g	Rate of heat generated [W]
l	Characteristic length [m]	$Q_{i \rightarrow j}$	Rate of heat transfer from i to j [W]
l_g	Characteristic length of heat flux in gas [m]	Q_r	Rate of heat transfer by radiation [W]
l_l	Characteristic length of heat flux in liquid [m]	Q_{rbb}	Rate of heat transfer by radiation of a black-body [W]
m	Mass [kg]	r	Radial coordinate [m]
\bar{m}	Effective mass [kg]	\tilde{r}	Average radius of particles [m]
M	Auxiliary parameter for indirect conduction [m]	\bar{r}	Radius of indirect conduction cylinder [m]
n_p	Number of particles [-]	r_c	Radius of the isothermal core of particle [m]
N_u	<i>Nusselt</i> number [-]	r_{ij}	Equivalent radius of the double tapered cone [m]
P_g	Pressure of gas [Pa]	r'_{ij}	Plane size to circumvent the inconsistency induced by different particle sizes [m]
P_r	<i>Prandtl</i> number [-]	r_{in}	Auxiliary parameters for indirect conduction [-]
Q	Net rate of heat transfer [W]		
Q_c	Rate of heat transfer by conduction [W]		
Q_{cpfp}	Rate of heat transfer by conduction due to contact particle-fluid-particle [W]		

Nomenclature

δ_f	Surrounding fluid layer of particle [m]	Λ	Auxiliary parameter for indirect conduction [-]
δ_i^{\min}	Auxiliary parameter for indirect conduction [m]	μ	Dynamic viscosity [Pa.s]
δ_i^{\max}	Auxiliary parameter for indirect conduction [m]	$\hat{\mu}$	Dynamic friction coefficient [-]
δ_n	Normal overlap [m]	μ_f	Dynamic viscosity of fluid [Pa.s]
$\dot{\delta}_n$	Normal overlap velocity [m/s]	μ_{fs}	Dynamic viscosity of fluid at surface temperature [Pa.s]
$\ddot{\delta}_n$	Normal overlap acceleration [m/s ²]	μ_g	Dynamic viscosity of gas [Pa.s]
δ_n^{\max}	Maximum normal overlap in a collision [m]	ν	Poisson ratio [-]
$\dot{\delta}_n^0$	Normal overlap velocity at impact [m/s]	ρ	Density [kg/(m ³)]
$\dot{\delta}_t$	Tangential relative velocity [m/s]	ρ_f	Density of fluid [kg/(m ³)]
Δ	Increment of a quantity [-]	σ	Stefan-Boltzmann constant [W/(m ² .K)]
∇	Gradient of a quantity [-]	τ	Rolling friction torque [N.m]
ε	Porosity (void fraction) [-]	φ	Filling angle of liquid bridge between particles [rad]
ϵ	Emissivity coefficient [-]	χ	Fraction of dissipation energy converted into heat [-]
ζ	Ratio of specific heat capacities [-]	ψ	partition coefficient of friction heat generation [-]
η	Parameter for the contribution of contact conduction [-]	ω	Molecular mean free-path [m]
θ	Angular coordinate [rad]	ω_r	Relative rotational velocity [rad/s]
θ_0	Angle between normal direction and tapered cone [rad]		
θ_1	Lower boundary angle for indirect conduction [rad]		
θ_2	Upper boundary angle for indirect conduction [rad]		
θ_c	Angle between normal direction and contact point [rad]		
λ	Parameter for particle temperature uniformity [-]		

Subscripts

cr	Critical value of a quantity
e	Surrounding environment property
eff	Effective property

Nomenclature

f Fluid property

g Gas property

i, j Particle indexes

k, l Max./Min. quantity between i and j

l Liquid property

p Particle property

$real$ Quantity computed with real material properties

s Surface property

w Wall property

Superscripts

t Time step index

Bibliography

Bibliography

1. Al-Arkawazi, S. Modeling the heat transfer between fluid-granular medium. *Applied Thermal Engineering*, vol. 128, pp. 696-705, 2018.
2. Amritkar A., Deb S. and Tafi D. Efficient parallel CFD-DEM simulations using OpenMP. *Journal of Computational Physics*, vol. 256, pp. 501-519, 2014.
3. Archard J.F. The temperature of rubbing surfaces. *Wear*, vol. 2, n. 6, pp. 438-455, 1959.
4. Batchelor G.K. and O'Brien R.W. Thermal or electrical conduction through a granular material. *Proceedings of the Royal Society of London. Series A, Mathematical and Physical Sciences*, vol. 355, n. 1682, pp. 313-333, 1977.
5. Botterill J.S.M., Salway A.G. and Teoman Y. The effective thermal conductivity of high temperature particulate beds - I: experimental determination. *International Journal of Heat and Mass Transfer*, vol. 32, n. 3, pp. 585-593, 1989.
6. Campbell C. Granular material flows – An overview. *Powder Technology*, vol. 162, n. 3, pp. 208-229, 2006.
7. Cengel Y.A. *Heat and mass transfer: a practical approach*. McGraw-Hill, New York, 2007.
8. Chan C.K. and Tien C.L. Conductance of packed spheres in vacuum. *Journal of Heat Transfer*, vol. 95, n.3, pp. 302-308, 1973.
9. Chaudhuri B., Muzzio F.J. and Tomassone M.S. Modeling of heat transfer in granular flow in rotating vessels. *Chemical Engineering Science*, vol. 61, n. 19, pp. 6348-6360, 2006.
10. Chen L., Wang C., Moscardini M., Kamlah M. and Liu S. A DEM-based heat transfer model for the evaluation of effective thermal conductivity of packed beds filled with stagnant fluid: Thermal contact theory and numerical simulation. *International Journal of Heat and Mass Transfer*, vol. 132, pp. 331-346, 2019.
11. Cheng G.J., Yu A.B. and Zulli P. Evaluation of effective thermal conductivity from the structure of a packed bed. *Chemical Engineering Science*, vol. 54, n. 19, pp. 4199-4209, 1999.
12. Cheng G.J., Yu A.B. Particle Scale Evaluation of the Effective Thermal Conductivity from the Structure of a Packed Bed: Radiation Heat Transfer. *Industrial & Engineering Chemistry Research*, vol. 52, n. 34, pp. 12202-12211, 2013.
13. Cheng G.J., Gan J., Xu D. and Yu A.B. Evaluation of effective thermal conductivity in random packed bed: Heat transfer through fluid voids and effect of packing structure. *Powder Technology*, vol. 361, pp. 326-336, 2020.
14. Crowe C.T. *Multiphase Flow Handbook*. CRC Press, Boca Raton, FL, 2006.
15. Cundall P.A. and Strack O.D.L. A discrete numerical model for granular assemblies. *Geotechnique*, vol. 29, pp. 47-65, 1979.
16. Dai W., Hanaor D. and Gan Y. The effects of packing structure on the effective thermal conductivity of granular media: A grain scale investigation. *International Journal of Thermal Sciences*, vol. 142, pp. 266-279, 2019.

Bibliography

17. Delvosalle C. and Vanderschuren J. Gas-to-particle and particle-to-particle heat transfer in fluidized beds of large particles. *Chemical Engineering Science*, vol. 40, no. 5, pp. 769-779, 1985.
18. Fan L. and Zhu C. *Principles of Gas-Solid Flows*. Cambridge University Press, Cambridge, UK, 1998.
19. Feng Y.T., Han K., Li C.F. and Owen D.R.J. Discrete thermal element modelling of heat conduction in particle systems: Basic formulations. *Journal of Computational Physics*, vol. 227, n. 10, pp. 5072-5089, 2008.
20. Gan J., Zhou Z. and Yu A. Particle scale study of heat transfer in packed and fluidized beds of ellipsoidal particles. *Chemical Engineering Science*, vol. 144, pp. 201-215, 2016.
21. Gunn D.J. Transfer of heat or mass to particles in fixed and fluidised beds. *International Journal of Heat and Mass Transfer*, vol. 21, n. 4, pp. 467-476, 1978.
22. Hahn M., Schwarz M., Kröplin B.-H. and Wallmersperger T. Discrete Element Method for the thermal field: Proof of concept and determination of the material parameters. *Computational Materials Science*, vol. 50, n. 10, pp. 2771-2784, 2011.
23. Hertz H. Über die Berührung fester elastischer Körper. *J. f. reine u. Angewandte Math.*, 92, pp. 156-171, 1882.
24. Hodowany J., Ravichandran G., Rosakis A.J. and Rosakis P. Partition of plastic work into heat and stored energy in metals. *Experimental Mechanics*, vol. 40, n. 2, pp. 113-123, 2000.
25. Holman J.P. *Heat Transfer*. McGraw-Hill, New York, 1981.
26. Hou Q.F., Kuang S.B. and Yu A.B. A DEM-based approach for analyzing energy transitions in granular and particle-fluid flows. *Chemical Engineering Science*, vol. 161, pp. 67-79, 2017.
27. Hu L., Zhu H. and Hua J. DEM simulation of energy transitions in a hammer mill: Effect of impeller configurations, agitation speed, and fill level. *Powder Technology*, vol. 394, pp. 1077-1093, 2021.
28. Incropera F.P. *Fundamentals of Heat and Mass Transfer*. John Wiley & Sons, 2006.
29. Jebahi M., André D., Terreros I. and Iordanoff I. *Discrete Element Method to Model 3D Continuous Materials*. John Wiley & Sons, 2015.
30. Johnson K.L. *Contact Mechanics*. Cambridge University Press, Cambridge, UK, 1985.
31. Kanuparthi S., Subbarayan G., Siegmund T., Sammakia B. An efficient network model for determining the effective thermal conductivity of particulate thermal interface materials. *IEEE Transactions on Components and Packaging Technologies*, vol. 31, n. 3, pp. 611-621, 2008.
32. Krause B., Liedmann B., Wiese J., Bucher P., Wirtz S., Piringer H. and Schere V. 3D-DEM-CFD simulation of heat and mass transfer, gas combustion and calcination in an intermittent operating lime shaft kiln. *International Journal of Thermal Sciences*, vol. 117, pp. 121-135, 2017.

Bibliography

33. Kunii D., Smith J.M. Heat transfer characteristics of porous rocks. *AIChE Journal*, vol. 6, n. 1, pp. 71-78, 1960.
34. Lambert M.A. and Fletcher L.S. Thermal contact conductance of spherical rough metals. *Journal of Heat Transfer*, vol. 119, n. 4, pp. 684-690, 1997.
35. Lattanzi A.M. and Hrenya C.M. A coupled, multiphase heat flux boundary condition for the discrete element method. *Chemical Engineering Journal*, vol. 304, pp. 766-773, 2016.
36. Lattanzi A.M. and Hrenya C.M. Indirect conduction in gas–solids systems: Static vs. dynamic effects. *AIChE Journal*, vol. 63, n. 10, 4685-4693, 2017.
37. Li J. and Mason D.J. A computational investigation of transient heat transfer in pneumatic transport of granular particles. *Powder Technology*, vol. 112, n. 3, pp. 273-282, 2000.
38. Li Y., Xu Y. and Thornton C. A comparison of discrete element simulations and experiments for ‘sandpiles’ composed of spherical particles. *Powder Technology*, vol. 160, n. 3, pp. 219-228, 2005.
39. Lu L., Morris A., Li T. and Benyahia S. Extension of a coarse grained particle method to simulate heat transfer in fluidized beds. *International Journal of Heat and Mass Transfer*, vol. 111, pp. 723-735, 2017.
40. Mokrani H and Bourouga B. Modèle de coefficient de partage du flux généré à une interface de contact électrothermique-approche microscopique en régime permanent. *12èmes Journées Internationales de Thermique*, vol. 426, 2005.
41. Molerus O. Heat transfer in moving beds with a stagnant interstitial gas. *International Journal of Heat and Mass Transfer*, vol. 4, pp. 4151-4159, 1997.
42. Morris A.B., Pannala S., Ma Z. and Hrenya C.M. A conductive heat transfer model for particle flows over immersed surfaces. *International Journal of Heat and Mass Transfer*, vol. 89, pp. 1277-1289, 2015.
43. Morris A.B., Pannala S., Ma Z. and Hrenya C.M. Development of soft-sphere contact models for thermal heat conduction in granular flows. *American Institute of Chemical Engineers Journal*, vol. 62, n. 12, pp. 4526-4535, 2016a.
44. Morris A.B., Ma Z., Pannala S. and Hrenya C.M. Simulations of heat transfer to solid particles flowing through an array of heated tubes. *Solar Energy*, vol. 130, pp. 101-115, 2016b.
45. Moscardini M, Gan Y., Papeschi S. and Kamlah M. Discrete element method for effective thermal conductivity of packed pebbles accounting for the Smoluchowski effect. *Fusion Engineering and Design*, vol. 127, pp. 192-201, 2018.
46. Moysey P.A. and Thompson M.R. Modelling the solids inflow and solids conveying of single-screw extruders using the discrete element method. *Powder technology*, vol. 153, n. 2, pp. 95-107, 2005.
47. Musser J.M.H. *Modeling of heat transfer and reactive chemistry for particles in gas-solid flow utilizing continuum-discrete methodology (CDM)*. PhD thesis, West Virginia University, 2011.

Bibliography

48. Nguyen V.D., Fortin J., Guessasma M., Bellenger E. and Cogné C. Thermomechanical modelling of friction effects in granular flows using the Discrete Element Method. *Journal of Mechanics of Materials and Structures*, vol. 4, n. 2, pp. 413-426, 2009a.
49. Nguyen V.D., Cogné C., Guessasma M., Bellenger E. and Fortin J. Discrete modeling of granular flow with thermal transfer: Application to the discharge of silos. *Applied Thermal Engineering*, vol. 29, n. 8-9, pp. 1846-1853, 2009b.
50. Nguyen V.D., Dufrénoy P. and Coorevits P. Simulation of energy dissipation and heat transfers of a braking system using the discrete element method: role of roughness and granular plateaus. *Journal of Heat Transfer*, vol. 142, n. 1, 012102, 2020.
51. Norouzi H.R., Zarghami R., Sotudeh-Gharebagh R. and Mostoufi N. *Coupled CFD-DEM Modeling: Formulation, Implementation and Application to Multiphase Flows*. Wiley, 2016.
52. Peng Z., Doroodchi E. and Moghtader, B. Heat transfer modelling in Discrete Element Method (DEM)-based simulations of thermal processes: Theory and model development. *Progress in Energy and Combustion Science*, vol. 79, 2020.
53. Quintana-Ruiz O.D. and Campello E.M.B. A coupled thermo-mechanical model for the simulation of discrete particle systems. *Journal of the Brazilian Society of Mechanical Sciences and Engineering*, vol. 42, n. 387, 2020.
54. Ranz W.E. and Marshall W.R. Evaporation from Drops. *Chemical Engineering Progress*, vol. 48, pp. 141-146, 1952.
55. Richard D., Iordanoff I., Renouf M. and Berthier Y. Thermal study of the dry sliding contact with third body presence. *Journal of Tribology*, vol. 130, n. 3, 031404, 2008.
56. Rojek J. Discrete element thermomechanical modelling of rock cutting with valuation of tool wear. *Computational Particle Mechanics*, vol. 1, pp. 71-84, 2014.
57. Rong D. and Horio M. DEM simulation of char combustion in a fluidized bed. In: *Proceedings of the second international conference on CFD in the minerals and process industries*, pp. 65-70, 1999.
58. Saxena S.C., Grewal N.S., Gabor J.D., Zabrodsky S.S. and Galershtein D.M. Heat transfer between a gas fluidized bed and immersed tubes. *Advances in Heat Transfer*, vol. 14, pp. 149-247, 1979.
59. Schlunder E.U. Heat transfer to moving spherical packings at short contact times. *International Chemical Engineering*, vol. 20, pp. 550-554, 1980.
60. Schlunder E.U. Particle Heat Transfer. In: *Proceedings of the 7th International Heat Transfer Conference*, pp. 195-211, 1982.
61. Siu W.W.M. and Lee S.W.-K. Transient temperature computation of spheres in three-dimensional random packings. *International Journal of Heat and Mass Transfer*, vol. 47, n. 5, pp. 887-898, 2004.
62. Soo S.L. *Fluid Dynamics of Multiphase Systems*. Blaisdell, Waltham, Massachusetts, 1967.
63. Sridhar M.R. and Yovanovich M.M. Elastoplastic contact conductance model for isotropic conforming rough surfaces and comparison with experiments. *Journal Heat Transfer*, vol. 118, n. 1, pp. 3-9, 1996.

Bibliography

64. Sun J. and Chen M.M. A theoretical analysis of heat transfer due to particle impact. *International Journal of Heat and Mass Transfer*, vol. 31, n. 5, pp. 969-975, 1988.
65. Sun Z., Zhu H. and Hua J. Granular flow characteristics and heat generation mechanisms in an agitating drum with sphere particles: Numerical modeling and experiments. *Powder Technology*, vol. 339, pp. 149-166, 2018.
66. Sun S., Deng X., Zhu W. and Yang X.O. Discrete element method simulation of energy dissipation mechanisms of HMX explosive particles under drop-weight impact. *Computational Materials Science*, vol. 203, 111129, 2022.
67. Terreros I., Iordanoff I., Charles J.L., Coupard D. and Tcherniaieff S. Discrete element method, a tool to investigate complex thermo mechanical behaviour: application to friction stir welding. *International Journal of Material Forming*, vol. 2, n. 1, pp. 573-576, 2009.
68. Timoshenko S. and Goodier J.N. *Theory of Elasticity*. McGraw-Hill, New York, 1951.
69. Tsory T., Ben-Jacob N., Brosh T. and Levy A. Thermal DEM-CFD modeling and simulation of heat transfer through packed bed. *Powder Technology*, vol. 244, pp. 52-60, 2013.
70. Váradi K., Néder Z. and Friedrich K. Evaluation of the real contact areas, pressure distributions and contact temperatures during sliding contact between real metal surfaces. *Wear*, vol. 200, n.1-2, pp. 55-62, 1996.
71. Vargas W.L. and McCarthy J.J. Heat conduction in granular materials. *AIChE Journal*, vol. 47, pp. 1052-1059, 2001.
72. Vargas W.L. and McCarthy J.J. Conductivity of granular media with stagnant interstitial fluids via thermal particle dynamics simulation. *International Journal of Heat and Mass Transfer*, vol. 45, n. 24, pp. 4847-4856, 2002.
73. Vargas W.L. *Discrete Modeling of Heat Conduction in Granular Media*. PhD thesis, University of Pittsburgh, 2002.
74. Vernotte P. Calcul numérique, calcul physique: Application à la thermocinétique. En vente au Service de documentation et d'information technique de l'aéronautique, 1956.
75. Voronoi M.G. Nouveaux applications des paramètres continus à la théorie des formes quadratiques. *Journal für die Reine und Angewandte Mathematik*, 134, 198-287, 1908.
76. Wakao N. and Kato K. Effective thermal conductivity of packed beds. *Journal of Chemical Engineering of Japan*, vol. 2, n. 1, pp. 24-33, 1969.
77. Wang S., Luo K., Hu C., Lin J. and Fan J. CFD-DEM simulation of heat transfer in fluidized beds: Model verification, validation, and application. *Chemical Engineering Science*, vol. 197, pp. 280-295, 2019.
78. Weisstein E.W. *Sphere-Sphere Intersection*. From MathWorld-A Wolfram Web Resource. <https://mathworld.wolfram.com/Sphere-SphereIntersection.html>

Bibliography

79. Wen C.Y. and Chang T.M. Particle-to-particle heat transfer in air-fluidized beds. In: *Proceedings of the International symposium on fluidization*, Eindhoven, pp. 491-505, 1967.
80. S. Whitaker. Forced convection heat transfer correlations for flow in pipes, past flat plates, single cylinders, single spheres, and for flow in packed beds and tube bundles. *AIChE Journal*, vol. 18, n. 2, pp. 361-371, 1972.
81. Wu S.M., Zhu H.P., Yu A.B. and Zulli P. Numerical investigation of crater phenomena in a particle stream impact onto a granular bed. *Granular Matter*, vol. 9, n. 1, pp. 7-17, 2007.
82. Yagi S. and Kunii D. Studies on effective thermal conductivities in packed beds. *American Institute of Chemical Engineers Journal*, vol. 3, n. 3, pp. 373-381, 1957.
83. Yang R.Y, Zou R.P. and Yu A.B. Voronoi tessellation of the packing of fine uniform spheres. *Physical Review E*, vol. 65, n. 4, 2002.
84. Yang W.J., Zhou Z.Y. and Yu A.B. Particle scale studies of heat transfer in a moving bed. *Powder Technology*, vol. 281, pp. 99-111, 2015.
85. Yun T.S. and Evans T.M. Three-dimensional random network model for thermal conductivity in particulate materials. *Computers and Geotechnics*, vol. 37, n. 7-8, pp. 991-998, 2010.
86. Zabrodsky S.S. *Hydrodynamics and Heat Transfer in Fluidized Beds*. MIT Press, Cambridge, MA, 1966.
87. Zhu H.P., Zhou Z.Y., Yang R.Y. and Yu A.B. Discrete particle simulation of particulate systems: Theoretical developments. *Chemical Engineering Science*, vol. 62, n. 13, pp. 3378-3396, 2007.
88. Zhou J.H., Yu A.B. and Horio M. Finite element modeling of the transient heat conduction between colliding particles. *Chemical Engineering Journal*, vol. 139, n. 3, pp. 510-516, 2008.
89. Zhou J.H., Yu A.B. and Zulli P. Particle scale study of heat transfer in packed and bubbling fluidized beds. *American Institute of Chemical Engineers Journal*, vol. 55, n. 4, pp. 868-884, 2009.
90. Zhou J.H., Yu A.B. and Zulli P. A new computational method for studying heat transfer in fluid bed reactors. *Powder Technology*, vol. 197, n. 1-2, pp. 102-110, 2010.
91. Zohdi T.T. A direct particle-based computational framework for electrically enhanced thermo-mechanical sintering of powdered materials. *Mathematics and Mechanics of Solids*, vol. 19, n. 1, pp. 93-113, 2013.